ChemComm

FEATURE ARTICLE

View Article Online
View Journal | View Issue

Cite this: *Chem. Commun.*, 2024, **60**, 14935

Bioinspired metal–organic frameworks for aqueous environment decontamination: from laboratory scale to real-world technologies

Cristina Negro,[a] Walter D. Guerra,[a] Donatella Armentano,[b] Jesús Ferrando-Soria,[a] Thais Grancha*[a] and Emilio Pardo*[a]

Received 14th October 2024,
Accepted 18th November 2024

DOI: 10.1039/d4cc05439c

rsc.li/chemcomm

Concerns regarding water contamination are escalating due to the increasing presence of all types of pollutants in water sources, which pose serious health risks to humans and wildlife, disrupt ecosystems, and compromise the safety of drinking water. Addressing water contamination requires stringent regulations and increased public awareness, but especially, it requires the development of highly effective new technologies to decontaminate those aquatic environments that have been already polluted over the past few decades. Since the emergence of metal–organic frameworks (MOFs), their use has been proposed in a multitude of fields, given their unique physicochemical properties, and one of the fields where a realistic application can be expected in the near future is water remediation. In particular, oxamidato-based biological MOFs (bioMOFs) have demonstrated, in recent years, unique properties such as extraordinary robustness, crystallinity and water- and pH-stability as well as very easy functionalisation, which situates them among the best adsorbents for this environmental purpose. In this review, we have summarised the most remarkable results of oxamidato-based bioMOFs in the field of water remediation. Moreover, on the basis of the reported results, we dare to suggest the real possibilities of application, in relevant real-world environments, for these and other MOFs, as well as the main obstacles that will need to be overcome, aiming to widening the range of applicability of MOFs and making solid headway towards sustainable development.

1. Introduction

Today's society faces a huge challenge due to the increasing presence of a wide diversity of both inorganic and organic pollutants. Among them, emerging pollutants,[1,2] such as heavy metals,[3] per- and polyfluoroalkyl substances (PFAS),[4] insecticides, pesticides, medical[5] or recreational[6] drugs, *etc.*, – arising from uses and customs of modern human activities (Fig. 1) – are of particular concern due to a certain lack of information about the harmful effects of these species as well as the most efficient approach to achieve their removal. Indeed, recent studies[2] confirm that these substances, which pose significant risks to aquatic ecosystems and human health, are often not fully removed by conventional wastewater treatment processes.[7,8] Their persistence and bioaccumulation potential can lead to long-term environmental impacts, affecting water quality and biodiversity. Addressing this issue requires the development of advanced treatment technologies and stricter regulatory frameworks to ensure the safety and sustainability of water resources.

In traditional water treatment plants,[9,10] water decontamination typically involves a series of steps: coagulation and flocculation (adding chemicals to form larger particles from small contaminants), sedimentation (allowing these larger particles to settle), filtration (passing water through sand, gravel, and activated carbon filters to remove remaining particles and chemicals), disinfection (using chlorine, chloramine, or UV light to kill pathogens), and sometimes advanced treatments like reverse osmosis or ozone treatment to remove specific contaminants and ensure water safety and quality. Among them, the adsorption step is crucial as it requires the sorbent material to be capable to sequestrate the soluble pollutants from the contaminated solutions. In fact, many studies demonstrate the difficulties water treatment plants face[7,8] in efficiently decontaminating various contaminants (especially emerging ones). In this regard, although activated carbon has traditionally been shown to be an excellent adsorbent material,[11] it is necessary to develop new materials that may have a greater affinity for emerging contaminants, considering the problems that wastewater treatment plants experiment dealing with these contaminants.

[a] *Instituto de Ciencia Molecular (ICMol), Universidad de Valencia, 46980 Paterna, Valencia, Spain. E-mail: thais.grancha@uv.es, emilio.pardo@uv.es*
[b] *Dipartimento di Chimica e Tecnologie Chimiche, Università della Calabria, 87036 Rende, Cosenza, Italy*

Fig. 1 Sources of groundwater contamination, arising from human activities, in the hydrologic cycle. This figure was image generated using Microsoft Designer.

Metal organic frameworks (MOFs)[12–14] are porous crystalline materials that may offer, in principle, certain advantages – among other remarkable properties – in water decontamination *versus* more traditional adsorbents.[15–17] In particular, MOFs permit a greater synthetic control on their functional empty space in terms of size, shape and, especially, the functionalities decorating their channels. This explains their fascinating host–guest chemistry,[18–21] and allows a fine-tuning of their affinity for the target contaminants, thus improving their water remediation properties. In addition, a particular class of MOFs, so-called multivariate MOFs[22–24] (MTV-MOFs), has emerged with great strength in the field of MOFs. MTV-MOFs – which maintain a general common backbone but multiple distinct organic functionalities – are particularly suitable for water remediation.[25–31] They offer the possibility to tune, in a rational manner, the multiple functionalities decorating their pores, envisaging a greater efficiency in capturing contaminants with various functional groups and, tentatively, the simultaneous capture of different contaminants.

Indeed, MOFs – and also a specific type of MOFs, formed by ligands derived from biomolecules and known as biological MOFs[32,33] (bioMOFs) – have been revealed as excellent adsorbent materials for the capture of a wide variety of inorganic[17,34,35] and organic contaminants.[25,27–31,36,37] However, despite these remarkable advances, MOFs have not yet achieved their implementation in real environments, such as waste treatment plants or smaller industrial devices.[38,39] This fact can be explained by a combination of factors such as the increased synthetic difficulty in preparing certain MOFs (many of which requiring solvothermal conditions), the difficulty in scaling up these materials,[40] their price per kg, especially when compared to the reference material (GAC = granular activated carbon), and the need to improve the mechanical properties of many MOFs, as well as their shaping into different composites,[41,42] which is a critical step aiming at real applications,[43] as it facilitates their integration into capture devices. In any case, the potential rewards in terms of selectivity and efficiency of MOFs in water remediation suggest that, once these difficulties are overcome, MOFs will be definitively established in the market.[43]

Finally, it also seems clear that once MOFs with outstanding capture properties are achieved, they need to be shaped[41,42] into robust hybrid composites, with improved mechanical properties and convenient handling, thus permitting their incorporation into current capture devices/treatment plants. In recent years, different works have been published in which MOFs have been shaped – with or without binders – to yield water remediation suitable materials such as pellets/granules, papers, membranes, foams or hollow structures.[41,42]

2. Oxamidato-based bioMOFs as suitable adsorbent materials

Among the plethora of MOF families reported to date, only a few seem to meet the requirements to compete with, and tentatively surpass, the adsorbent properties of the reference materials currently in use (*i.e.* granular activated carbons).[44] Specifically, the ideal MOF, that would enable a step forward in capture processes associated with water treatment must necessarily meet a series of unique requirements.[25] For example, it must exhibit permanent porosity, be stable in aqueous media (preferably at different pH levels), and allow for precise control of the size and shape of its pores/cavities, as well as the functional groups decorating them to enhance affinity for target contaminants.[25]

2.1. General characteristics and advantages of amino acid oxamidato-based bioMOFs for water remediation

Among the variety of reported MOFs, oxamato- and oxamidato-based MOFs[45,46] have shown more than suitable, fulfilling satisfactory all the above described requirements. Additionally, they exhibit other unique properties, such as great robustness and high crystallinity, which, in the past, have allowed for the determination of the structure of host–guest aggregates,[47,48] even after several post-synthetic processes.[49–55] This point is highly relevant as – unlike the vast majority of MOFs – offers the possibility to unveil the host–guest interactions,[47,48] responsible for the capture of the contaminants, permitting a positive feedback between structure and functionality, and consequently, to develop novel and more efficient adsorbents. Moreover, oxamidato-based MOFs syntheses, based on direct precipitation methods[45,46] (*vide infra*), can be easily scaled-up, and the resulting MOFs can be also shaped,[45,46] which are important features thinking on real world applications.[39]

Of all the reported oxamato and oxamidato-based MOF families, one stands out as particularly suitable for environmental remediation. Specifically, it is a family of amino acid-derived oxamidato-based biological MOFs (bioMOFs), which exhibits a series of unique characteristics in addition to those shared with other oxamidato-based MOFs mentioned above (*vide infra*). Oxamidato-based

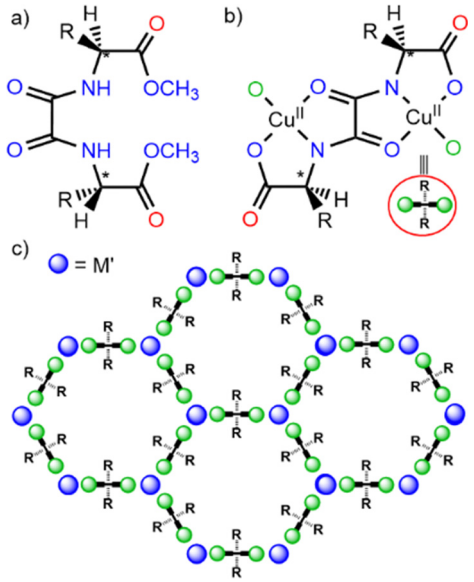

Scheme 1 Chemical structures of the amino acid-based oxamidato ligands (a) and dicopper(II) precursor complexes (b), as well as a schematic representation of the bioMOF hexagonal network emphasizing the position of the amino acid residues (c). R represent the amino acid residues decorating the channels.

bioMOFs represent a versatile and extensive class of isoreticular porous coordination polymers. Their common crystal structures typically consist of a chiral, honeycomb-like 3D network, built from calcium(II) or strontium(II) ions coordinated with copper(II) centres (Scheme 1). Overall, these structures feature functional hexagonal channels, with pore sizes ranging from approximately 0.3 nm to 1 nm, making them ideal candidates for applications involving molecular sieving and selective adsorption.

From a topological point of view, the framework can be described by an **acs** uninodal sixfold-connected motif. This topology is constructed from *trans*-oxamidato-bridged dicopper(II) units (Scheme 1b), {Cu_2^{II}[(*S*,*S*)-ligand]}, which serve as linkers between Ca^{II} or Sr^{II} nodes through their carboxylate functionalities (Scheme 1c). The neighbouring Cu^{2+} and Cu^{2+}/Ca^{2+} ions are further interconnected *via* aqua or hydroxo groups in a μ_3-bridging configuration, present in a 1 : 2 statistical distribution, thus forming robust yet flexible frameworks.

Indeed, one of the defining characteristics of this class of MOFs is their exceptional intrinsic flexibility,[56] which is predominantly localised within the pore structure. This flexibility allows the frameworks to adapt their conformation depending on the size, shape, and chemical properties of the guest molecules. Notably, the variety of amino acid-derived moieties within the structure provides additional functional diversity (Scheme 1c). This adaptability, paired with a strong and resilient backbone, allows oxamidato-based bioMOFs to withstand harsh environmental conditions while remaining versatile enough to engage in selective interactions with various guest molecules. In other words, the synergistic combination of structural robustness and dynamic flexibility imparts these materials with unique properties, enhancing their potential for applications in the area of water remediation.

In this context, the most relevant features of oxamidato-based bioMOFs, as well as their advantages against other MOFs, are summarised below.

2.1.1. Water and pH-stability of oxamidato-based bioMOFs. Since their emergence, MOFs have shown application in very diverse fields. However, their use in water remediation is more recent.[25–31,36,37,57–61] The main reason for such delay is, undoubtedly related with the low water stability that most of the early examples of MOFs exhibited,[62,63] as a consequence of the relatively weak strength of their coordination bonds. To overcome this limitation, various strategies were proposed, in the following years, to increase the water stability of MOFs, such as strengthening these bonds – by selecting appropriate ligands and/or increasing the oxidation state of the metals or introducing hydrophobic units into their network. As a result, there is now a fairly wide range of MOFs that are stable in water, and even at different pH levels.[62,63] This aspect is not only crucial for developing materials that can be used for decontaminating aquatic environments but also for enabling their reuse multiple times, as has been demonstrated (Section 3).

Oxamato and oxamidato-based MOFs are well-known for their high-water stability. In fact, some of them are well-known for being capable to host very large number of water molecules even exhibiting sponge-like behaviour[64,65] or properties associated to transport with water molecules, such as proton conductivity.[66] For example, our first reported example of oxamidato-based bioMOF, with the natural amino acid L-alanine and with formula {$Ca^{II}Cu_6^{II}$[(*S*,*S*)-alamox]$_3$(OH)$_2$(H$_2$O)}·32H$_2$O[66] (**Cu_6CaAla**) (where (*S*,*S*)-alamox = bis[(*S*)-alanine]oxalyl diamide), exhibited high thermal and water and basic media stability (Fig. 2). Indeed, this bioMOF did not show any apparent degradation after being soaked for one month in a pH = 14 aqueous solutions.

2.1.2. Outstanding crystallinity in harsh conditions. Elucidation of the crystal structure of many MOFs, through

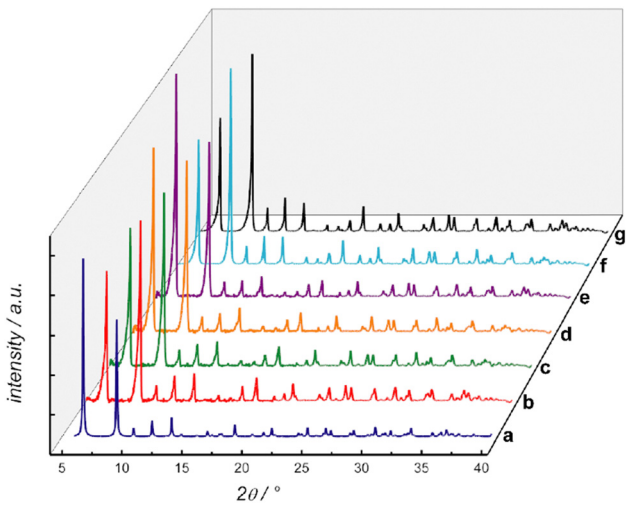

Fig. 2 (a) Calculated PXRD pattern profile of **Cu_6CaAla**. Variable temperature XRD patterns of the activated phase of **Cu_6CaAla** at 298 (b), 343 (c), 353 (d), and 370 K (e). PXRD pattern profiles of 1 after proton conduction measurements (f) and after 1 month immersed in a pH = 14 aqueous solution (g) at RT. This figure is reproduced with permission from ref. 66, copyright ACS 2016.

single-crystal X-ray diffraction (SCXRD) analysis, has constituted a challenge since the advent of these porous materials, as this requires high quality crystals that not always can be obtained.[67,68] Therefore, other techniques like powder X-ray diffraction,[69] X-ray absorption techniques[70] and even high-resolution electron microscopies[71] are often required. In this context, oxamidato-based MOFs have not only shown enough crystallinity to elucidate their crystal structures through SCXRD but, in addition, such crystallinity is maintained even after the application of harsh consecutive post-synthetic methods, and thus, the crystal structures of different host–guest aggregates, such as metal nanoclusters,[50,53,54,56,72] supramolecular complexes[73,74] or organic molecules[21,55] (Fig. 3) embedded within the channels of the MOFs, have been repeatedly obtained, in recent years, with oxamato- and oxamidato-based MOFs.

In this sense, SCXRD can be a powerful tool in water remediation, by unveiling the crystal structures of the host–guest aggregates after the capture processes and allowing to visualise the host–guest interactions governing them, with the aim of optimising the design process of new MOFs with increasingly better capture properties.

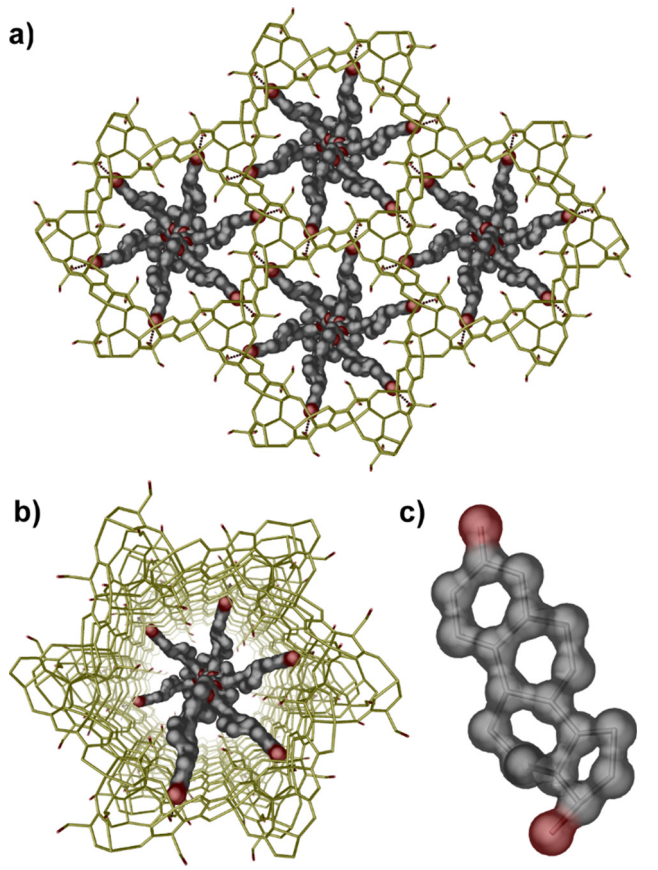

Fig. 3 (a) View along the crystallographic *c* axis of the porous structure of bioMOF **Cu$_6$CaSer**, prepared from the natural amino acid L-serine, encapsulating the hormone 17-β-estradiol. (b) Perspective view of one single-channel of the hybrid host–guest material. (c) Chemical structure of 17-β-estradiol. The networks are depicted as gold sticks whereas guest molecules are represented as red (oxygen), green (chloride), blue (nitrogen) and gray (carbon) stick/solid surfaces, respectively.

2.1.3. Functionalization "a-la-carte" of the bioMOFs' empty space. Among the different families of oxamato- and oxamidato-based MOFs reported to date, oxamidato-based bioMOFs, derived from amino acids, are particularly suitable for water remediation taking into account the wide variety of residues that can be incorporated, rationally, into the channels of these bioMOFs. Thus, depending on the amino acid used to construct the bioMOF, different factors, such as functionality, flexibility, charge, and even the hydrophobicity or hydrophilicity of the pores, which largely determines the capture properties of the material, can be controlled. For example, **Cu$_6$CaAla** showed a honeycomb-like hexagonal 3D $Ca^{II}Cu^{II}_6$ open-framework, with the methyl groups from the amino acid residues pointing towards the centre of the channels (Scheme 1a). As all oxamidato-based bioMOFs of this family (Table 1) are isoreticular, by selecting appropriate amino acids the functionalities decorating the channels of the resulting bioMOF can be rationally controlled (see below synthetic strategy, Scheme 1b and c) and thus, other properties such as gas adsorption or selectivity, and, of course, their capture properties, can be modified/enhanced. Moreover, the heterogeneity of channels functionalities can be increased, by selecting amino acids of different nature, constituting the so-called multivariate bioMOFs (MTV-bioMOFs, Fig. 4).

This exquisite functionalisation of the bioMOF channels lies at the origin of the capture properties of this family of bioMOFs, as we can control the functional groups decorating the channels in order to enhance the affinity for the target contaminant. The adsorption mechanisms driving these capture processes rely on various supramolecular interactions between the amino acid-derived functional groups of the bioMOFs and the target contaminants. These interactions include a large variety of the non-covalent interactions, *i.e.* hydrogen bonding, van der Waals forces, π–π stacking, and σ-hole interactions, as elucidated through SCXRD analysis (see Section 3).

2.2. Synthetic strategy

Oxamidato-based bioMOFs are usually synthesised following rational programmed methods based on the "complex-as-ligand" approach,[45,46] which allow for a greater synthetic control of MOF structure, compared to solvothermal ones. This methodology consists on the sequential step by step construction of the bioMOF, firstly with the preparation of the bis[amino acid]oxalyl diamide ligand (Scheme 1a and Table 1), followed by the synthesis/isolation of a precursor complex (Scheme 1b), and finally, the direct precipitation of the bioMOF in water under ambient conditions, without any control of parameters such as pH, temperature, ionic strength, *etc.*, by reacting the precursor with a second metal (Scheme 1c). In so doing, a family of isoreticular bioMOFs, with a wide variety of amino acids, such as L-alanine, L-valine, L-leucine, L-histidine, L-serine, L-threonine, L-methionine or *S*-methyl-L-cysteine, can be obtained, with the corresponding residues decorating their channels (Fig. 4).

Thus, a fine tuning of the size, shape and, especially the functionality and hydrophobicity/hydrophilicity of the channels is achieved. In addition, the synthetic approach above described constitutes a very suitable pathway to construct, rationally, MTV-bioMOFs by combining the appropriate

Table 1 Oxamidato-based bioMOFs described in this work and removal efficiency for different target contaminants

Name	Chemical formula	Amino acids involved [percentage]	Target contaminant [maximum recovery (%)]	Ref.
Cu_6CaAla	$\{Ca^{II}Cu^{II}_6[(S,S)\text{-alamox}]_3(OH)_2(H_2O)\}\cdot 32H_2O$	L-Alanine [100%]	—	66
Cu_6CaMet	$\{Ca^{II}Cu^{II}_6[(S,S)\text{-methox}]_3(OH)_2(H_2O)\}\cdot 16H_2O$	L-Methionine [100%]	$HgCl_2$ [99.5%] CH_3Hg [99.0%]	75
Cu_4Met	$\{Cu^{II}_4[(S,S)\text{-methox}]_2\}\cdot 5H_2O$	L-Methionine [100%]	$HgCl_2$ [99.7%]	76
$Cu_6CaMecys$	$\{Ca^{II}Cu^{II}_6[(S,S)\text{-Mecysmox}]_3(OH)_2(H_2O)\}\cdot 16H_2O$	*S*-Methyl-L-cysteine [100%]	$HgCl_2$ [99.9%]	77
$Cu_6CaMet/Mecys$	$\{Ca^{II}Cu^{II}_6[(S,S)\text{-methox}]_{1.5}[(S,S)\text{-Mecysmox}]_{1.5}(OH)_2(H_2O)\}\cdot 38H_2O$	L-Methionine [50%] *S*-Methyl-L-cysteine [50%]	$Pb(NO_3)_2$ [98.2%]	78
Cu_6CaSer	$\{Ca^{II}Cu^{II}_6[(S,S)\text{-serimox}]_3(OH)_2(H_2O)\}\cdot 39H_2O$	L-Serine [100%]	Methylene blue [93.3%] Auramine O [92.0%] Pyronine Y [91.7%] Brilliant green [96.1%]	79
Cu_6SrMet	$\{Sr^{II}Cu^{II}_6[(S,S)\text{-methox}]_3(OH)_2(H_2O)\}\cdot 16H_2O$	L-Methionine [100%]	Methylene blue [100%] Auramine O [100%] Pyronine Y [100%] Brilliant green [100%]	80
$Cu_6SrMet/Mecys$	$\{Sr^{II}Cu^{II}_6[(S,S)\text{-methox}]_{1.5}[(S,S)\text{-Mecysmox}]_{1.5}(OH)_2(H_2O)\}\cdot 36H_2O$	L-Methionine [50%] *S*-Methyl-L-cysteine [50%]	Acetamiprid [100%] Thiacloprid [100%]	81
Cu_6SrSer	$\{Sr^{II}Cu^{II}_6[(S,S)\text{-serimox}]_3(OH)_2(H_2O)\}\cdot 38H_2O$	L-Serine [100%]	Ciprofloxacin [99.0%] Amoxicillin [100%] Clindamyzin [98.1%] Ceftriaxone [100%]	82
Cu_6SrMet/Ser	$\{Sr^{II}Cu^{II}_6[(S,S)\text{-methox}]_{1.5}[(S,S)\text{-serimox}]_{1.5}(OH)_2(H_2O)\}\cdot 12H_2O$	L-Methionine [50%] L-Serine [50%]	Ciprofloxacin [99.4%] Amoxicillin [100%] Clindamyzin [97.4%] Ceftriaxone [100%]	82
Cu_6CaMet/Ser	$\{Ca^{II}Cu^{II}_6[(S,S)\text{-methox}]_{1.5}[(S,S)\text{-serimox}]_{1.5}(OH)_2(H_2O)\}\cdot 16H_2O$	L-Methionine [50%] L-Serine [50%]	$HgCl_2$ [99.7%] $Pb(NO_3)_2$ [99.2%] $TlNO_3$ [99.4%] Methylene blue [100%] Auramine O [99.8%] Pyronine Y [99.7%] Brilliant green [100%]	83

percentages of different precursors at the same time. In this way, we can rationally design ambivalent channels with a desired affinity for different types of contaminants or even capturing challenging pollutants, such as those possessing both polar and non-polar groups (amphiphilic contaminants).

Regarding, the potential for real applications of these bioMOFs in water remediation, oxamidato-based bioMOFs can be easily obtained in a multigram scale, which contrasts to that observed for other MOFs synthesised using solvothermal procedures. Indeed, they are obtained by direct precipitation in water under ambient conditions. This facilitates to scale-up their synthesis to a hundred of grams or kilograms scale, which is a key step for the mass production of MOFs, aiming at their application in real environments. In this context, the shaping/processing of MOFs also constitutes a crucial step, prior to be incorporated in capture devices, where oxamidato-based bioMOFs have also demonstrated their suitability (*vide infra*).

3. Specific applications of oxamidato-based bioMOFs in water remediation

3.1. Oxamidato-based bioMOFs for inorganic contaminants removal

3.1.1. Mercury. One of the greatest challenges the world faces today is the increasing heavy metal pollution caused by industrial activities and/or accidental discharge. In particular, mercury – which is considered by the World Health Organization (WHO)[84] as one of the top ten chemicals or groups of chemicals of major public health concern – is widespread in the environment due to its very easy air and water transportation, as well as its long atmospheric lifetime. As a consequence, high concentrations of mercury and derivatives can be found not only in fish,[85] but also in agricultural crops.[86] Once in the environment, mercury can be transformed by bacteria into methylmercury, which is considered even more hazardous since it bioaccumulates in living beings due to its lower solubility in water.

MOFs have been mainly studied for their ability to adsorb mercury,[17,34,35,87,88] and the specific focus on methylmercury uptake has been much less studied, despite its unique toxicity and bioaccumulation. Chiefly, two main strategies for mercury removal with MOFs have been proposed: (i) cation exchange with the counter-cations – in case of anionic MOFs – located in the pores, which have shown no preferential adsorption, as it is based on charge effects, and thus, with no possible application for real complex matrices,[17,34] and (ii) pre- or post-synthetically functionalisation with sulphur atoms the organic linkers of MOFs, based on the well-known affinity of sulphur atoms towards soft metal ions,[89] which have revealed as more rational and efficient manners to capture mercury.

In this context and having in consideration the above-mentioned features of oxamidato-based bioMOFs, firstly, we

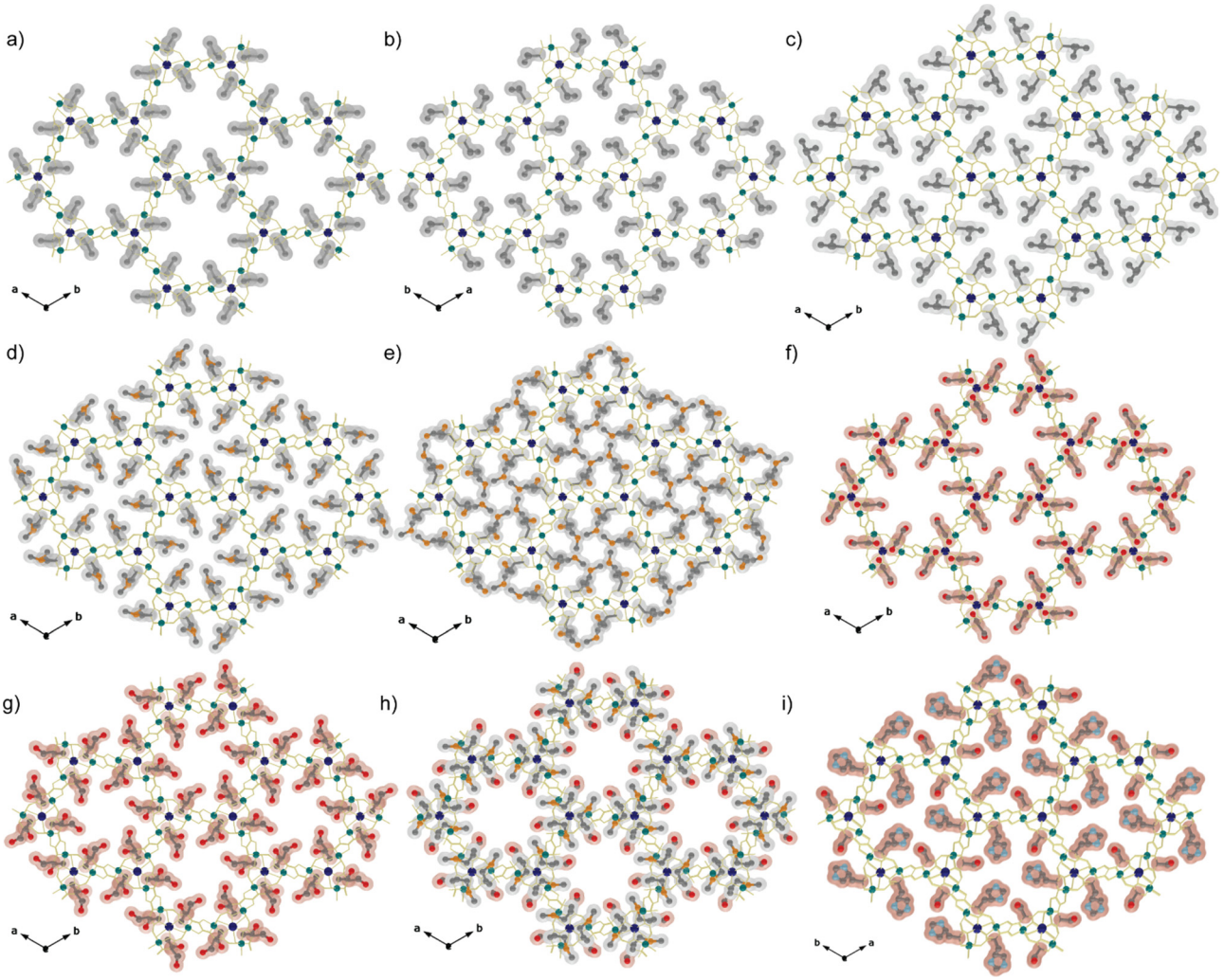

Fig. 4 Selected examples of recently synthesized oxamidato-based bioMOFs (a)–(g) and MTV-bioMOFs (h) and (i) prepared from the following amino acids: L-alanine (a), L-valine (b), L-leucine (c), *S*-methyl-L-cysteine (d), L-methionine (e), L-serine (f), L-threonine (g), L-methionine/L-serine (red) (h) and L-histidine (blue)/L-serine (i). Grey and red surfaces are used to emphasise the hydrophobicity and hydrophilicity, respectively, of the corresponding amino acid residues.

focused our attention on a robust and water-stable, heterobimetallic calcium(II)/copper(II) bioMOF, which was synthesised by using a ligand derived from the natural amino acid L-methionine.[49,75] This bioMOF with the formula $\{Ca^{II}Cu^{II}_6[(S,S)\text{-methox}]_3(OH)_2(H_2O)\}\cdot 16H_2O$ (**Cu_6CaMet**) (where methox = bis[(*S*)-methionine]oxalyl diamide), features functional channels decorated with thioalkyl chains (Fig. 4e and 5), which – on the basis of the well-known affinity of mercury for sulphur atoms[89] – situates **Cu_6CaMet** as a very appealing candidate for mercury removal. **Cu_6CaMet** crystallises in the chiral $P6_3$ space group and consists of an uninodal **acs** chiral net built by calcium(II) vertexes and *trans* oxamidato-bridged dicopper(II)units, $\{Cu^{II}_2[(S,S)\text{-methiox}]\}$, which act as linkers between the Ca^{II} ions through the carboxylate groups. In the resulting porous net, the functional flexible ethylthiomethyl chains of the amino acid-derived ligand remain confined in hexagonal channels. When tested towards mercury species uptake, **Cu_6CaMet** showed high adsorption performance, achieving maximum recoveries of 900 ($HgCl_2$) and 166 mg (CH_3HgCl) per g. Such a high loading of $HgCl_2$ was one of the highest reported, to date,[25] for a MOF, and constituted a benchmark value for MOFs. Also, it is worth mentioning that **Cu_6CaMet** was the first known MOF for CH_3HgCl uptake, and that only very few examples have been reported since then.[75]

These uptakes were reversible and selective towards $HgCl_2$ and CH_3HgCl, which make of this material a potential sorbent. Thus, aiming at assessing its applicability in real world decontamination processes, extruded pellets were obtained by combining polycrystalline powder of **Cu_6CaMet** with the commercial polymer Matrimid5218. In this shape, kinetic profile of each mercury removal process was established. The experimental results showed that this hybrid material adsorbed both mercury salts in a very fast, selective, and reversible manner. Remarkably, the $HgCl_2$ and CH_3HgCl concentrations in water were reduced from dangerous 10 ppm to extremely low levels of about 5 and 27 ppb after capturing 99.95% and 99.0% of the

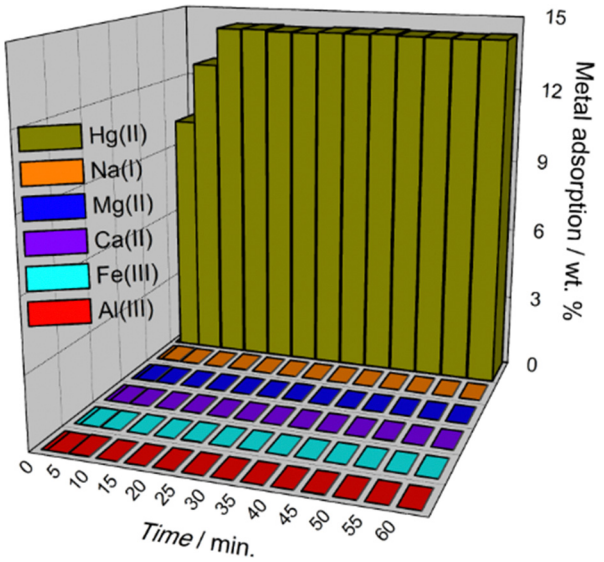

Fig. 5 Kinetic profile of the selective Hg(II) recovery by bioMOF **Cu_6CaMet** represented as metal adsorption (wt%) *vs.* time in the presence of other interfering metal cations.

dissolved $HgCl_2$ and CH_3HgCl salts (Fig. 5), respectively, which is within the permissible limits for Hg^{2+} ions in potable water.[84]

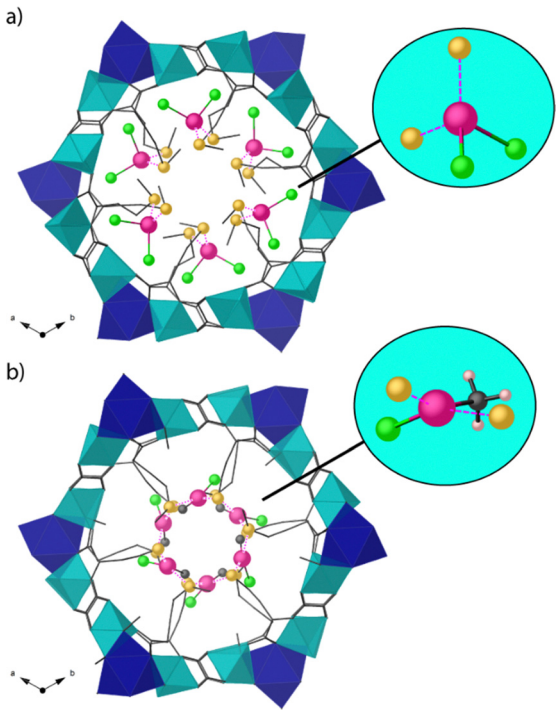

Fig. 6 Perspective views of one single channel of bioMOF **Cu_6CaMet** after capturing **$HgCl_2$** (a) and **CH_3HgCl** (b). Copper and calcium atoms are represented by cyan and blue polyhedra respectively. Mercury and chloride atoms are depicted as purple and green spheres, whereas sulphur and carbon atoms from the residues are shown as yellow spheres and grey sticks. This figure is adapted with permission from ref. 75, copyright Wiley & Sons 2016.

Noteworthy, substantial knowledge on the attachment and conformation of these mercury species inside the pores of a MOF could be shed, for the first time, thanks to the great crystallinity that **Cu_6CaMet** shows, even upon loading conditions, which allowed the resolution of crystalline structures through SCXRD (Fig. 6). The chemical environment inside the voids of **Cu_6CaMet**, provided by the highly flexible ethylthiomethyl chains of methionine ligands, reminds that of the mercury reductase (MR) enzyme (Fig. 6a). Both systems having in common an intriguing structural adaptability capable to recognise and immobilise mercury species through S···Hg interactions.

Despite **Cu_6CaMet** showed benchmark uploads for mercury species among MOFs, we wanted to accomplish much lower mercury levels and in a faster manner, that is a better efficiency. The followed strategy was to design a bioMOF displaying thioalkyl functionalities (as **Cu_6CaMet**), but targeting more constricted pores. Thus, reaction of the previously used oxamidato ligand derived from the natural amino acid L-methionine towards Cu^{II} ions, afforded a new microporous bioMOF featuring narrow square-shaped channels decorated with thioalkyl chains.[76] The bioMOF of formula $\{Cu^{II}_4[(S,S)\text{-methox}]_2\}\cdot 5H_2O$ (**Cu_4Met**) showed lower maximum loading capacity than **Cu_6CaMet** (280 mg per g of bioMOF), but much better kinetic profile as well as efficiency. The moderate loading capacity of **Cu_4Met** is due to its narrower pores and overall lower porosity. On the contrary, when mercury uptake kinetics of **Cu_4Met** was investigated, an outstanding decrease of $HgCl_2$ concentration from 10 ppm to below 2 ppb was achieved in 15 min, thus revealing an exceptional removal behaviour and affording values within the permissible limits in drinking water.[84]

In **Cu_4Met**, as in **Cu_6CaMet**, the affinity binding was ensured by resemblance with MR enzyme, whereas selectivity and kinetics were controlled by the size and shape of the pores.

In the light of such promising results on mercury decontamination, we could say that oxamidato-based bioMOFs represent firm candidates for water remediation technologies. However, MOFs powders present some inherent drawbacks, such as difficult handling or losses/leakages of fine powders, when searching for industrial uses. Thus, with the purpose of going one step forward, we explored the mercury decontamination performance of **Cu_6CaMet** and a brand-new bioMOF (**Cu_6CaMecys**) (Fig. 4d) as fillers into mixed-matrix membranes (MMMs) in batch conditions (see Section 4 for further details), and eventually, into a device designed for decontamination in dynamic flux.[77] Since thioalkyl arms decorating the pores of the bioMOF have shown essential for providing the sulphur binding sites to anchor mercury species, we chose **Cu_6CaMet** and tested a new bioMOF derived from the amino acid *S*-methyl-L-cysteine with formula $\{Ca^{II}Cu^{II}_6[(S,S)\text{-Mecysmox}]_3(OH)_2(H_2O)\}\cdot 16H_2O$ (**Cu_6CaMecys**), (where Mecysmox = bis[(*S*-)methylcysteine]oxalyl diamide). Both **Cu_6CaMet** and **Cu_6CaMecys** are isoreticular and their flexible thioalkyl arms point inwards the hexagonal channels, being the only difference between them the empty space in the voids. Ethylthiomethyl groups in **Cu_6CaMet** are bulkier than methythiomethyl ones in **Cu_6CaMecys**, showing the last a higher porosity. Mercury uptake

capacity of **Cu_6CaMecys** was assessed showing capability to reduce the Hg^{2+} concentration from 10 ppm to 4.6 ppb, close enough to acceptable limits for drinking water, in 4 h. Being then proved both **Cu_6CaMet** and **Cu_6CaMecys** as effective adsorbents, two MMMs using Matrimid5218 as polymer matrix were prepared, **matrimid@Cu_6CaMet** and **matrimid@Cu_6CaMecys**. The Hg^{2+} removal efficiency of the two MMMs was studied by both static adsorptions in batch and dynamic adsorption during permeation, adapting a microfiltration test cell, thus recirculating the contaminated solutions through the bioMOF-MMMs *via* a peristaltic pump. From all the results shed in this work, here we highlight those achieved in the more challenging conditions: very low concentrated solutions of Hg^{2+} prepared with oligo mineral water, which contain other metal cations – that may interfere adsorption process – in higher concentration than mercury. Thus, in static conditions, Hg^{2+} concentration dropped from 370 ppb to 1.85 and 1.20 ppb, after 72 h, with **matrimid@Cu_6CaMet** and **matrimid@Cu_6CaMecys**, respectively. In dynamic conditions, Hg^{2+} concentration decreased from 330 to 1.78 and 1.26 ppb, after 48 h, with **matrimid@Cu_6CaMet** and **matrimid@Cu_6CaMecys**, respectively. Achievements in this work were two-folded: (i) a novel device consisting of the recirculation and microfiltration of contaminated water through the bioMOF-MMMs was developed and it satisfactorily performed and, (ii) in both static and dynamic decontamination regimes, achieved Hg^{2+} concentrations were below limits for drinking water established by the U.S. Environmental Protection Agency (EPA, <2 ppb).

3.1.2. Lead. Lead is a very harmful metal that has been widely used, leading to significant environmental pollution and health issues in many regions around the globe. Specially, the main source of lead-contamination is the corrosion of household plumbing systems, *e.g.* Flint water crisis.[90] Lead is a cumulative toxin – considered also of the top ten chemicals of major public health concern–, that impacts various body systems, including the nervous, blood, digestive, cardiovascular, and renal systems.[91] The maximum contaminant level goal, established by the United States Environmental Protection Agency (EPA) is 0 μg L^{-1}.[92] However, this result is not viable with existing technologies – benchmark phosphate dosage only is able to reach 15 μg L^{-1}. Thus, so far, the maximum allowed levels for lead, established by the EPA and the U.S. Food and Drug Administration (FDA), are 10 and 5 μg L^{-1} (for bottled water), respectively.

Capacity of MOFs for Pb^{2+} capture has been investigated and some MOFs have performed quite well. However, the minimum Pb^{2+} levels reached are above the accepted limits for drinking water. Having our family of bioMOFs demonstrated such good mercury removal capacity, based on Coordination Chemistry basic principles, we proposed them for lead decontamination. In this work,[78] we targeted Pb^{2+} uptake by using a MTV-bioMOF, which is derived from the two amino acids L-methionine and L-methyl-cysteine, since both bear thioether residues and, therefore, sulphur atoms which show great affinity for Pb^{2+}. The MTV-bioMOF of formula $\{Ca^{II}Cu^{II}_6[(S,S)\text{-methox}]_{1.5}[(S,S)\text{-Mecysmox}]_{1.5}(OH)_2(H_2O)\}\cdot 38H_2O$ (**Cu_6CaMet/Mecys**) is isoreticular to the aforementioned family (Fig. 4). Thus, **Cu_6CaMet/Mecys** features hexagonal functional channels. But, in this case, decorated with two types of thioether groups, being either $-CH_2CH_2SCH_3$ or $-CH_2CH_3$ (methionine and methyl-cysteine, respectively), pointing toward the accessible void spaces and creating a favourable and confined space to trap Pb^{2+} species.

The removal behaviour of MTV-bioMOF **Cu_6CaMet/Mecys**, in the shape of polycrystalline sample (50 mg) was evaluated towards an aqueous solution of $Pb(NO_3)_2$ (1 ppm). We found that **Cu_6CaMet/Mecys** could drastically reduce Pb^{2+} concentration to less than 5 ppb, sufficiently close to acceptable limits for drinking bottled water. Remarkably, not only robustness of **Cu_6CaMet/Mecys** was proven after the capture experiments, but also Pb^{2+} uptake could be followed and unambiguously unveiled by SCXRD. The crystal structure of **Pb@Cu_6CaMet/Mecys** confirmed that lead ions are trapped inside the pores of **Cu_6CaMet/Mecys** stabilised by $S\cdots Pb^{2+}$ linkage. An auxiliary interaction of Pb^{2+} with oxygen atoms belonging to oxamidato ligands from the MTV-bioMOF was also revealed, likely contributing to stabilising the metal ions in the confined spaces.[78,93]

3.2. Oxamidato-based bioMOFs for organic contaminants removal

3.2.1. Organic dyes. Dyes are mainly used to colour fabrics and other materials, such as leather, fur, hair, waxes, and plastics. Specially, textile industry consumes more than 10 000 tons of dyes, and the washing processes of textiles generate a large volume of liquid waste that contains dyes and pigments.[94] Unfortunately, the entire dying process releases dye-containing effluents, which eventually, end up at remote areas through contaminated streams and oceans. This is especially alarming since the emissions all over the world are found increasing at a rapid rate.[95] Contamination of aquatic ecosystems with organic dyes represents a severe environmental problem, having a negative impact on the quality of aquatic ecosystems, inhibiting plants and algae photoactivity and representing a health threat for fish and human, as a consequence of their teratogenic, mutagenic and carcinogenic character.[96]

Having shown oxamidato-based bioMOFs great capabilities for heavy metals capture and having in consideration the different functionalities decorating the pores that this family of bioMOFs has, we logically aimed at testing them towards the capture of organic nature contaminants, starting with organic dyes. Crystallographic evidence shown so far on the effective interactions between the amino acid residues decorating the pores of our bioMOFs' family and contaminants, led us to think that these could also play a key role in the capture of dyes. Therefore, we set two main objectives: achieve the selective capture of dyes from water and solve the crystal structure of bioMOFs containing dyes. So, information on the effective host–guest interactions could be drawn enabling the rationalisation and design of bioMOF structures with optimal removal behaviour, especially at relevant very low concentration (parts per million levels).

In our first related work,[79] we targeted the adsorption of four well known organic dyes Pyronin A (PY), Auramine O (AO),

Brilliant Green (BG) and Methylene Blue (MB). As sorbent, we used an oxamidato-bioMOF derived from the ligand L-serine (Fig. 4f) with formula $\{Ca^{II}Cu^{II}_6[(S,S)\text{-serimox}]_3(OH)_2(H_2O)\}\cdot 39H_2O$ (**Cu_6CaSer**) (where serimox = bis[(*S*-)serine]oxalyl diamide).[79] **Cu_6CaSer** displays the typical honeycomb six-connected 3D calcium(II)–copper(II) network of this family, and features highly hydrophilic hexagonal channels (pore size of *ca.* 0.9 nm) decorated with hydroxyl groups from L-serine. **Cu_6CaSer** performed quite well towards the capture of dyes, achieving maximum uploads of 772.8, 575.7, 1269.7 and 739.8 mg per g for PY, AO, BG and MB, respectively. Aiming at the potential applicability of **Cu_6CaSer** and following similar strategy described above, we also prepared pellets of **Cu_6CaSer** combined with the polymer Matrimid5218 (**matrimid@Cu_6CaSer**). These pellets (50 mg) were immersed in a solution containing the four dyes in a concentration like that found in real industrial wastewater (10 ppm each dye) and prepared with mineral water-containing ions naturally present in water. Remarkably, **matrimid@Cu_6CaSer** adsorbed the four dyes in a quite fast and very effective manner, thus removing almost completely the dyes from the solution (86.1–91.7%) in 6 h (Fig. 7a).

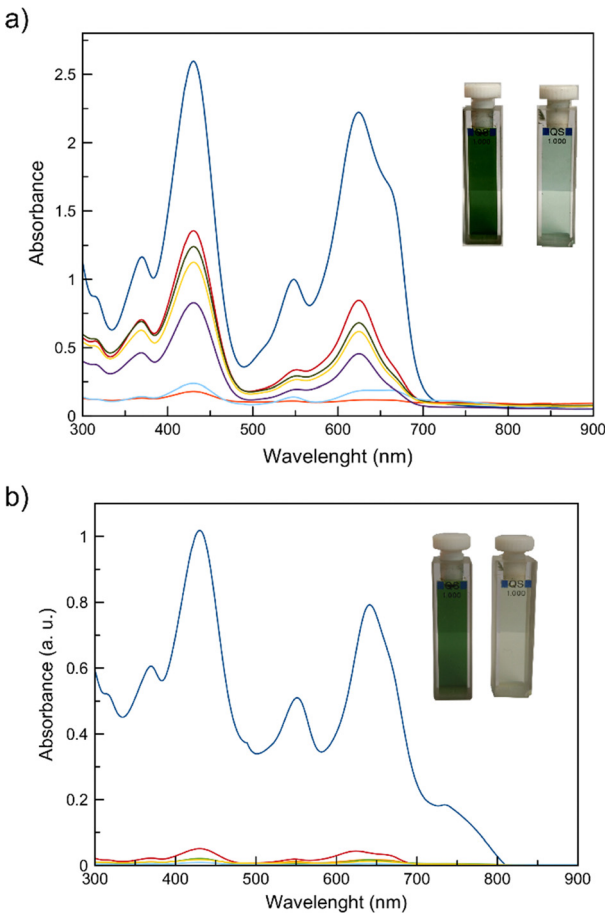

Fig. 7 Comparative evolution with time of the UV-Vis absorption spectra of a multidye aqueous solution containing 10 ppm of Auramine O, Brilliant green, Methylene blue and Pyronin Y in the presence of bioMOF **Cu_6CaSer** (a) and **Cu_6SrMet** (b). Blue: t = 0; red: t = 1 min; yellow: t = 5 min; orange t = 30 min; light blue t = 360 min; green: t = 720 min. The photographs show the colours of the solutions at the beginning (left) and after only one minute of exposure of the multidye solution with the corresponding bioMOF (right). This figure is adapted with permission from ref. 79 and 80, copyright ACS and Wiley & Sons 2018.

Moreover, the high crystallinity of **Cu_6CaSer** allowed to resolve the crystal structure of the host–guest aggregates, hereafter named **PY@Cu_6CaSer**, **AO@Cu_6CaSer** (Fig. 8), **BG@Cu_6CaSer** and **MB@Cu_6CaSer** and revealed valuable information (Fig. 8). Firstly, all four bioMOF structures were maintained after the dye insertion, which demonstrates the stability and robustness of oxamidato-based bioMOFs. Secondly, the main interactions governing the dye anchoring were similar for all four dyes and consisted of H-bonds or weak C–H···O interactions mediated by the arms of the serine derivative. Thirdly, while in **PY@Cu_6CaSer** and **AO@Cu_6CaSer** prevailed interactions of dye molecules directly with the net of **Cu_6CaSer**, in **BG@Cu_6CaSer** and **MB@Cu_6CaSer** the lattice water molecules confined in the pores were non-innocent participants, and also contributed to the stabilisation of BG and MB. With this work, we not only demonstrated the decontamination power of the family of oxamidato-bioMOFs, but also got unprecedented snapshots of the real host–guest interactions that govern the dye uptake.

Despite the good performance of **Cu_6CaSer** towards dye removal, we still wanted to further explore the potential of other members of our family of bioMOFs. At this respect, along the course of our investigations, we have found that sulphur atoms play a key role in several recognition processes through supramolecular interactions. Among these, we inferred that sulphur σ-hole interactions may have a prominent role in the capture of organic molecules, such as dyes.[80] Thus, we prepared a new bioMOF, isostructural to **Cu_6CaMet**, but containing Sr(II) instead of Ca(II) acting as the nodes in the uninodal **acs** chiral net, with formula $\{Sr^{II}Cu^{II}_6[(S,S)\text{-methox}]_3(OH)_2(H_2O)\}\cdot 16H_2O$[80] (**$Cu_6$SrMet**).

Maximum loading capacity of **Cu_6SrMet** was tested towards dyes PY, AO, BG and MB, founding uptakes of 542.6, 598.9, 786.8 and 554.0 mg per g, respectively. These are lower than those reported for **Cu_6CaSer** (L-serine derivative bioMOF), probably due to the lower pore size that **Cu_6SrMet** displays. Later, like in previous works, we tested the kinetics of **Cu_6SrMet** in the shape of extruded pellets (Matrimid5218). A solution containing the

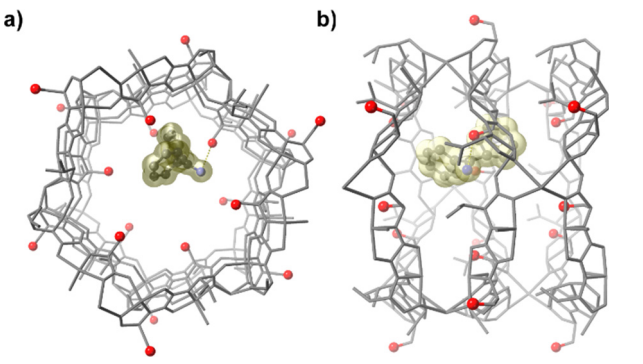

Fig. 8 Top (a) and side (b) views of a fragment of a single channel of bioMOF **Cu_6CaSer** encapsulating capture Auramine O molecules. The networks are depicted as grey sticks whereas the guest organic dye is represented as spheres and yellow surface.

four dyes PY, AO, BG and MB in 10 ppm concentration was prepared (Fig. 7b). As a novelty, we used real water from Turia river (Valencia, Spain) to prepare the dye-contaminated solutions, aiming at reproducing more realistic conditions. The obtained kinetic profile evidenced the efficient and fast adsorption of all four dyes, reaching almost 100% of removal after only 1 min. This contrasts with the serine-based bioMOF, which needed more than 6 h to reach the same capture efficiency. In addition, we were also able to resolve the crystal structure of **Cu_6SrMet** containing the different dyes trapped in the pores, hereafter named **PY@Cu_6SrMet**, **AO@Cu_6SrMet**, **BG@Cu_6SrMet** and **MB@Cu_6SrMet**. This allowed the atomically-precise visualisation of the main host–guest interactions, likely at the origin of the efficient capture of pollutant dyes. So, the main host–guest interactions were assured by sulphur atoms, directly interacting either with Cl^- anions in **PY@Cu_6SrMet**, **AO@Cu_6SrMet** and **MB@Cu_6SrMet** or with aromatic rings *via* the low-lying σ* orbitals of the C–S bond (σ-hole interaction).[80]

3.2.2. Pesticides. The contribution of pesticides to boost global agricultural output is substantial. However, improper use has posed harmful environmental impacts. A large portion of pesticides – or their metabolites when degraded by the ecosystem – seeps into groundwater or flows into surface waters through runoff, threatening the whole ecosystem and, eventually, water supplies and human health.[97] Among them, neonicotinoids[98] (NEOs) are a widely used type of insecticides that spread easily due to their moderate solubility in water. In fact, The European Environment Agency (EEA) claimed that imidacloprid was one of the pesticides found exceeding the quality threshold at 25% of the water monitoring sites.[99] Therefore, monitoring and eliminating pesticides from water sources is a critical global priority.

Aiming at proposing oxamidato-bioMOFs as an alternative to more traditional materials used for pesticides removal, in a recent work, we tested their great host–guest capabilities shown so far toward the adsorption of different NEOs. Among the bioMOFs explored, specially three of them, **Cu_6CaMet** and **Cu_6CaMecys** and a novel MTV-bioMOF with formula $\{Sr^{II}Cu^{II}_6[(S,S)\text{-methox}]_{1.5}[(S,S)\text{-mecysmox}]_{1.5}(OH)_2(H_2O)\}\cdot 36H_2O$ (**Cu_6SrMet/Mecys**),[81] showed great removal performance of imidacloprid, thiamethoxam, clothianidin, acetamiprid and thiacloprid.

Initially, the efficiency on the NEOs capture was evaluated toward aqueous solutions containing the five NEOs at different relevant concentrations. For the evaluation, solid phase extraction (SPE) devices were prepared by packing 25 mg of the corresponding bioMOF into empty propylene cartridges (1 mL volume). Thus, the contaminated solutions were percolated through them and the corresponding analyses carried out. Overall, **Cu_6CaMet**, **Cu_6CaMecys** and **Cu_6SrMet/Mecys** captured very efficiently thiacloprid and acetamiprid and, moderately well, clothianidin, imidacloprid and thiamethoxam. Interestingly, **Cu_6SrMet/Mecys** showed the best performance even at very low concentration (0.1 mg L^{-1}), achieving removal values of 71 (thiamethoxam), 86 (clothianidin), 86 (imidacloprid), 100 (thiacloprid) and 99% (acetamiprid). **Cu_6CaMet** and **Cu_6CaMecys** showed more modest uptake of clothianidin, imidacloprid and thiamethoxam, but outstanding uptake of thiacloprid and acetamiprid, achieving removal values of 95, 93% (**Cu_6CaMet**) and 91, 96% (**Cu_6CaMecys**), respectively.

Then, we wanted to further prove our materials at more realistic conditions, using complex matrices, looking for real-world applications. In so doing, capture experiments were performed with real water samples taken from the Turia River (Valencia, Spain) – with possible competing species–, which were spiked at 5 mg L^{-1} with each of the five NEOs. Excellent removal efficiencies were found, especially for acetamiprid and thiacloprid, achieving values of 96, 99% (**Cu_6CaMet**), 77, 95% (**Cu_6CaMecys**) and 100% (**Cu_6SrMet/Mecys**), respectively. For clothianidin, imidacloprid and thiamethoxam, efficiencies of 21–45% (**Cu_6CaMet**), 34–42% (**Cu_6CaMecys**) and 58–78% (**Cu_6SrMet/Mecys**) were found. The reusability of the bioMOF-containing cartridges was also assessed and it could be observed that, at least for 10 cycles, the three bioMOFs maintained the efficiency of the removal of the five NEOs.[81]

Crystallographic data of MTV-bioMOF **Cu_6SrMet/Mecys** containing acetamiprid (Fig. 9) and thiacloprid revealed that both guest molecules are encapsulated in the nanopores and simultaneously recognised by the thioether arms of the methyl-cysteine and methionine residues (Fig. 9b), being the most relevant stabilising forces the ones assured by the sulphur atoms interacting with nitrile groups or with Cl atoms as electron donors (Fig. 9b). The simultaneous contribution of both type of amino acid residues – with similar functionalisation but different electron density – seems to optimise the accommodation of guests inside the channels of bioMOF *versus* those bioMOFs derived from single methionine or single methyl-cysteine (**Cu_6CaMet** and **Cu_6CaMecys**).

3.2.3. Antibiotics. Antibiotics are a class of pharmaceutical drugs widely used to prevent and treat bacterial infections. Even though their development has been key to the existing wellbeing in societies, their excessive and improper use has created a significant risk to both the balance of ecosystems and human health, contributing to the emergence of antibiotic resistance genes (ARGs).[100] Antibiotics are commonly found in surface waters across the globe, and are frequently detected in rivers, lakes, oceans, and even in drinking water. Despite the magnitude of this problematic, there is a lack of specific water decontamination protocols for the elimination of antibiotics at sewage plants. Among the technologies investigated so far, traditional porous solids have been exploratory considered (*i.e.* activated carbon and zeolites). Thus, based on the reported successful decontamination performance of the family of oxamidato-bioMOFs and on the work developed by us, where they were used for extraction, detection and quantification of vitamins,[101] we proposed our materials for the efficient removal of antibiotics from water. Noteworthy, previously, scarce examples of MOFs with this purpose could be found in the literature. Besides, no MTV-MOFs performing towards antibiotic capture had been published so far.

In this publication, we described the antibiotic removal behaviour of the already reported **Cu_6SrMet** (derived from L-methionine), and novel isostructural bioMOF derived from

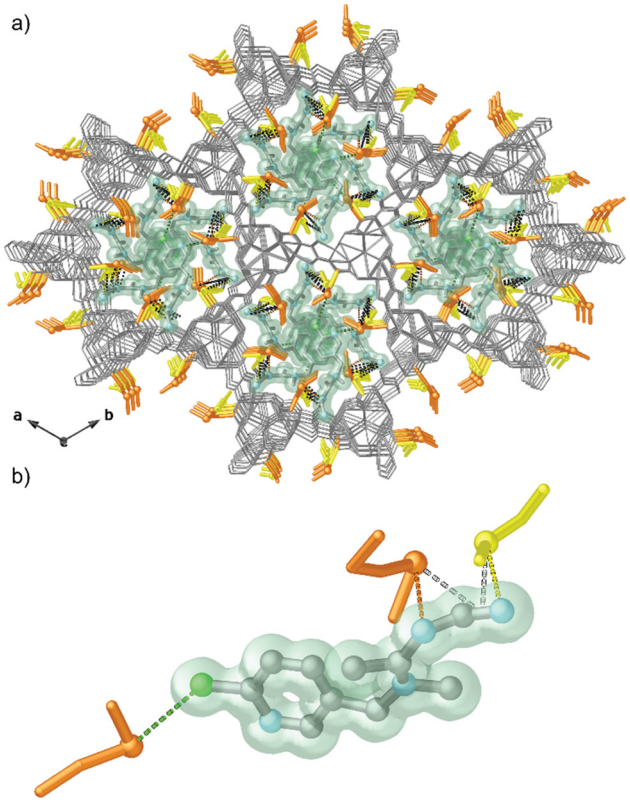

Fig. 9 (a) Perspective view, in the *ab* plane, of the porous structure of bioMOF **Cu$_6$SrMet/Mecys** with acetamiprid molecules embedded. (b) Detailed view of the captured acetamiprid molecules emphasising the host–guest interactions with thioether groups from L-methionine and *S*-methyl-L-cysteine amino acids. Guest molecules are represented as green solid surfaces for the sake of clarity. This figure is adapted with permission from ref. 81, copyright ACS 2021.

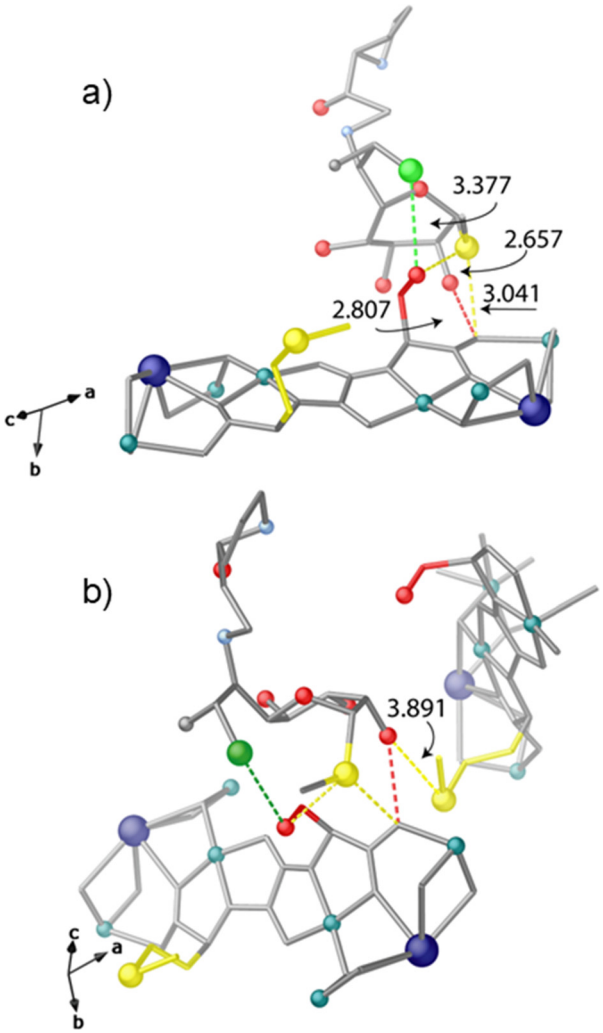

Fig. 10 (a) Details of crystal structure of bioMOF **Cu$_6$SrMet/Ser** with clindamycin molecules embedded underlining the interactions involving hydroxyl groups of serine moieties and chlorine and sulphur atoms of guest molecules in the cooperative network of host–guest interactions. (b) Details of crystal structure of the same host–guest aggregate underlining the interactions involving sulphur atom of methionine moieties and oxygen atoms of guest molecules. This figure is adapted with permission from ref. 82, copyright ACS 2023.

L-serine (**Cu$_6$SrSer**) and isostructural MTV-bioMOF (**Cu$_6$SrMet/Ser**) containing 50% of thioether and 50% alcohol residues from L-methionine and L-serine (Fig. 4h), respectively, whose chemical formulas are $\{Sr^{II}Cu^{II}_6[(S,S)\text{-serimox}]_3(OH)_2(H_2O)\}\cdot 38H_2O$ (**Cu$_6$SrSer**) and $\{Sr^{II}Cu^{II}_6[(S,S)\text{-methox}]_{1.5}[(S,S)\text{-serimox}]_{1.5}(OH)_2(H_2O)\}\cdot 12H_2O$ (**Cu$_6$SrMet/Ser**).[82] These bioMOFs, in the shape of SPE sorbents (*vide supra*), were tested toward four widely used antibiotics ciprofloxacin, amoxicillin, clindamycin (Fig. 10) and ceftriaxone, each one belonging to a different representative family.[82]

The capture experiments were performed using environmental matrices, such as real water samples from Albufera natural park (Valencia, Spain) and a sewage treatment plant (Paterna, Spain), which were further spiked using mixtures of the four antibiotics at two concentrations (5 and 25 mg L^{-1}). Overall, the three materials showed very high removal efficiency (*ca.* 100%) for all four antibiotics in both concentrations and in a single loading step. This represented an astounding result – considering that adsorption process took place in 30 s and that we were using environmental matrices–, and positioned **Cu$_6$SrMet**, **Cu$_6$SrSer** and **Cu$_6$SrMet/Ser** among the best-performing materials. The difference in the performance of **Cu$_6$SrMet**, **Cu$_6$SrSer** and **Cu$_6$SrMet/Ser** lies on their reusability. Whilst **Cu$_6$SrMet** and **Cu$_6$SrSer** presented a very limited reusability, the MTV-bioMOF **Cu$_6$SrMet/Ser** showed an impressive removal efficiency of 99% after 15 cycles. Remarkably, **Cu$_6$SrMet/Ser** started outperforming activated carbon (benchmark material) after the 10th reuse (Table 2).[82] Last but not least, SCXRD afforded unique insights about the host–guest interactions governing the capture processes by means of the resolution of the host–guest adsorbate with clindamycin molecules hosted in the channels of **Cu$_6$SrMet/Ser** (Fig. 10).

3.3. Simultaneous removal of inorganic and organic contaminants

Up to this point, our results have validated the synthetic strategy that we follow. We have demonstrated that we can elegantly tailor the pore functionalisation, through the somehow wise choice of the starting amino acid, depending on the

final application that we are pursuing. For example, **Cu_6CaMet** exhibited great performance toward Hg^{2+} capture, thanks to the well-known affinity that sulphur atoms from the methionine residue show by soft metals. Following the same rationale, **Cu_6CaSer** achieved great success on dye removal thanks to the hydroxyl groups that serine amino acid display, which stablished powerful interactions with the dyes. Bearing this in mind, and with the final goal of achieving porous materials with optimal dual decontamination performance, we prepared the MTV-bioMOF of formula, $\{Ca^{II}Cu^{II}_6[(S,S)\text{-methox}]_{1.5}[(S,S)\text{-serimox}]_{1.5}(OH)_2(H_2O)\}\cdot 30H_2O$[83] (**$Cu_6$CaMet/Ser**, Fig. 11a), to target the simultaneous uptake of both organic and inorganic contaminants from water.

Firstly, removal performances toward organic dyes and metal cations were assessed separately. Therefore, an aqueous multidye solution containing the four dyes PY, AO, BG and MB (10 ppm each dye) was prepared and **Cu_6CaMet/Ser** (50 mg) was soaked in the shape of polycrystalline sample. The adsorption of all four dyes occurred in a very rapid manner; after 15 min 92.0 (PY), 92.1 (AO), 96.0 (BG) and 90.6% (MB) removal efficiency was achieved. These findings were particularly significant considering that such cleaning efficiency was achieved at very low concentration – similar to that found in real industrial wastewater. Later, the efficiency and selectivity of **Cu_6CaMet/Ser** toward the removal of toxic soft heavy metals was examined. Hence, polycrystalline sample of **Cu_6CaMet/Ser** (50 mg) was immersed in an aqueous solution containing $Hg(NO_3)_2$, $Pb(NO_3)_2$ and $TlNO_3$ (1 ppm each metal ion) where other salts were also added ($NaNO_3$, KNO_3, $Mg(NO_3)_2$, $Ca(NO_3)_2$, $Ni(NO_3)_2$ and $Cu(NO_3)_2$). After 2 h, concentrations of 7 (Hg^{2+}), 65 (Pb^{2+}) and 365 ppb (Tl^{+}), were found, whilst concentrations of the rest of metal cations remained 1 ppm, thus confirming the high removal efficiency and selectivity of **Cu_6CaMet/Ser**. Remarkably, all these results achieved by **Cu_6CaMet/Ser** (dyes and heavy metal removal), improved those already reported by **Cu_6CaMet** and **Cu_6CaSer** (*vide supra*) – taking into account that **Cu_6CaMet/Ser** only bears 50% hydroxyl groups and 50% thioether groups. The reason behind such improvement could be the cooperative manner in which both alcohol and thioether arms work. Therefore, despite hydroxyl groups were reported to stablish the more stabilising interactions with dyes, also thioether arms have shown good performance and are playing a role in the dye immobilisation. Besides, likely, despite sulphur atoms from thioether arms showed optimal affinity towards heavy metal ions, interactions with the oxygen atoms from hydroxyl group are non-negligible.

Table 2 Comparative efficiency and reuses for bioMOFs **Cu_6SrMet**, **Cu_6SrSer** and **Cu_6SrMet/Ser** and activated carbon

Reuses	Cu_6SrMet	Cu_6SrSer	Cu_6SrMet/Ser	Activated carbon
1st	100.0	91.6	98.9	97.9
3rd	84.1	55.7	99.6	99.1
5th	45.2	38.3	99.7	99.4
7th	25.4	42.3	100.0	100.0
10th	31.1	33.6	99.5	93.1
15th	28.0	32.5	99.0	93.0

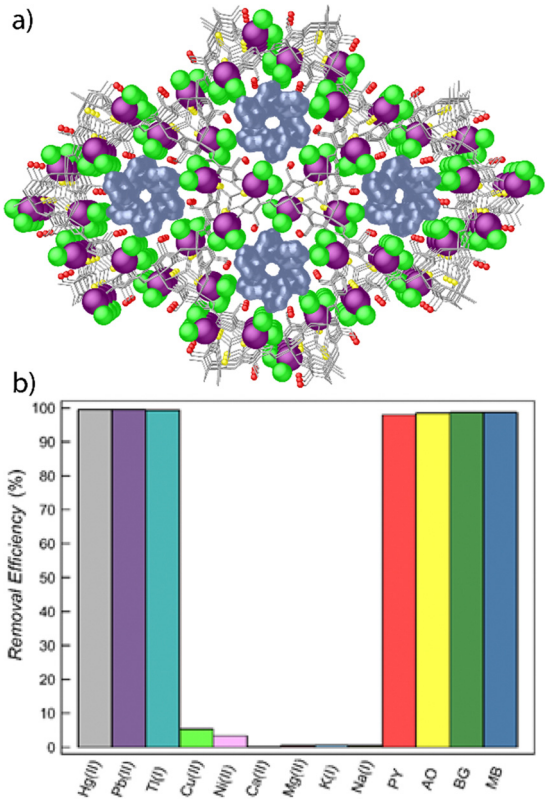

Fig. 11 (a) Details of crystal structure of MTV-bioMOF **Cu_6CaMet/Mecys** after the simultaneous capture of HgCl2 and methylene blue. Mercury and chlorine atoms are represented by magenta and green spheres, respectively, whereas methylene blue molecules are represented as blue surfaces. (b) Maximum recovery (after 6 h) of both inorganic and organic contaminants. This figure is adapted with permission from ref. 83, copyright ACS 2019.

Secondly, after such promising individual results, **Cu_6CaMet/Ser** was tested toward the simultaneous removal of both type of contaminants. To this end, aqueous solutions containing 1 ppm of $Hg(NO_3)_2$, $Pb(NO_3)_2$ and $TlNO_3$, $NaNO_3$, KNO_3, $Mg(NO_3)_2$, $Ca(NO_3)_2$, $Ni(NO_3)_2$ and $Cu(NO_3)_2$ and 10 ppm of PY, AO, BG and MB were prepared. Then, 50 mg of **Cu_6CaMet/Ser** were soaked in the solution under stirring. Analysis of the results revealed and excellent removal performance (Fig. 11b). Moreover, the removal efficiencies were slightly enhanced in comparison with the individual experiments, especially those of metal ions. In the case of dyes removal, after 15 min 90.1 (PY), 96.3 (AO), 92.3 (BG) and 92.3% (MB) uptake was achieved. The metal ion concentrations after 2 h were 6.0 (Hg^{2+}), 4.9 (Pb^{2+}) and 123 ppb (Tl^{+}). In order to be completely sure than **Cu_6CaMet/Ser** performed better than the corresponding monovariated-bioMOFs **Cu_6CaMet** and **Cu_6CaSer**, the above mentioned experiments were also run for a physical mixture of **Cu_6CaMet** (25 mg) and **Cu_6CaSer** (25 mg). We observed that this showed an approximately 15 and 20% worse efficiency for the removal of inorganic and organic contaminants, respectively.

Secondly, after such promising individual results, **Cu_6CaMet/Ser** was tested toward the simultaneous removal of both

type of contaminants. To this end, aqueous solutions containing 1 ppm of $Hg(NO_3)_2$, $Pb(NO_3)_2$ and $TlNO_3$, $NaNO_3$, KNO_3, $Mg(NO_3)_2$, $Ca(NO_3)_2$, $Ni(NO_3)_2$ and $Cu(NO_3)_2$ and 10 ppm of PY, AO, BG and MB were prepared. Then, 50 mg of **Cu_6CaMet/Ser** were soaked in the solution under stirring. Analysis of the results revealed and excellent removal performance (Fig. 11b). Moreover, the removal efficiencies were slightly enhanced in comparison with the individual experiments, especially those of metal ions. In the case of dyes removal, after 15 min 90.1 (PY), 96.3 (AO), 92.3 (BG) and 92.3% (MB) uptake was achieved. The metal ion concentrations after 2 h were 6.0 (Hg^{2+}), 4.9 (Pb^{2+}) and 123 ppb (Tl^{+}). In order to be completely sure than **Cu_6CaMet/Ser** performed better than the corresponding monovariated-bioMOFs **Cu_6CaMet** and **Cu_6CaSer**, the above mentioned experiments were also run for a physical mixture of **Cu_6CaMet** (25 mg) and **Cu_6CaSer** (25 mg). We observed that this showed an approximately 15 and 20% worse efficiency for the removal of inorganic and organic contaminants, respectively.

Finally, with the aim to unlock the snapshots of the dual capture process, we underwent the dual capture process into single crystals of **Cu_6CaMet/Ser**. This MTV-bioMOF revealed robust enough to stand the loading conditions, and the structural elucidation through SCXRD afforded unprecedented insight. To the best of our knowledge, this was the first crystal structure of an adsorbate with guests of different nature confined together within functional pores. Best quality crystals for resolution were those of **(MB)·$HgCl_2$@Cu_6CaMet/Ser**, isomorph of **Cu_6CaMet/Ser** confirming the preservation of the 3D network of the hosting matrix after capture. The crystal structure revealed $HgCl_2$ molecules hosted in the hexagonal pores of **Cu_6CaMet/Ser**, recognised by the thioether arms of the methionine residues and stabilised by S···Hg interactions. MB molecules where also trap in the hexagonal pores sharing space with $HgCl_2$, being packed *via* hydrogen bond interactions with both serine arms and other dye molecules. Interestingly, interactions between organic and inorganic pollutants were also found. These last may explain the improved results of the simultaneous contaminant capture in comparison with individual uptake experiments.

4. Processing of oxamidato-based bioMOFs

In light of all these results, the great efficiency, versatility, and selectivity of oxamidato-based bioMOFs, derived from amino acids, in capturing a wide range of organic and inorganic contaminants is clearly evident and reflects the great potential of this family of bioMOFs in water remediation. However, it is clear that further efforts are required in order to facilitate their application in real-world environments. In particular, processing oxamidato-based bioMOFs is crucial in order to shape the polycrystalline powders – obtained in chemical synthesis – into composites that could be, tentatively, incorporated in scalable capture devices.

In this sense, processing polycrystalline powders into composites, with appropriate mechanical properties and maintaining the reported capture properties, that can be effectively used as filters for an efficient decontamination in a continuous flow constitutes a clear step forward in the field. This strategy has been successfully started to be explored with oxamidato-based bioMOFs, with the preparation of bioMOF-based mixed matrix membranes (MMMs-bioMOFs) (Fig. 12)[77] for the removal of $HgCl_2$ in batch and dynamic conditions (see Section 3.1.1).

For example, we have anticipated, in Section 3, that bioMOFs derived from amino acids L-methionine and *S*-methyl-L-cysteine, **Cu_6CaMet** and **Cu_6CaMecys** – whose polycrystalline powders had exhibited extraordinary $HgCl_2$ capture properties (see Section 3) – could be also successfully integrated within porous organic polymers, yielding a type of hybrid material, so-called bioMOF-based mixed matrix membranes (MMM-bioMOFs) (Fig. 12).[77] Both MMM-bioMOFs exhibited, as their ancestor polycrystalline samples, high efficiency and selectivity in the removal of Hg^{2+} from contaminated aqueous solutions reaching a Hg^{2+} concentration below 2 ppb, which is within the acceptable limits for drinking water. This capture was not only carried out in a static regime but also in a continuous regime were contaminated solutions passed through membranes in a continuous manner. Thus, MMM-bioMOFs could be even incorporated within a lab-scale capture device (Scheme 2), consisting in a peristaltic pump capable to recirculate Hg^{2+} contaminated aqueous solution through the membranes, which exhibited excellent capture performances for small volumes of water.[77]

Aiming at developing more hybrid materials with similar capture properties but enhanced mechanical properties, we

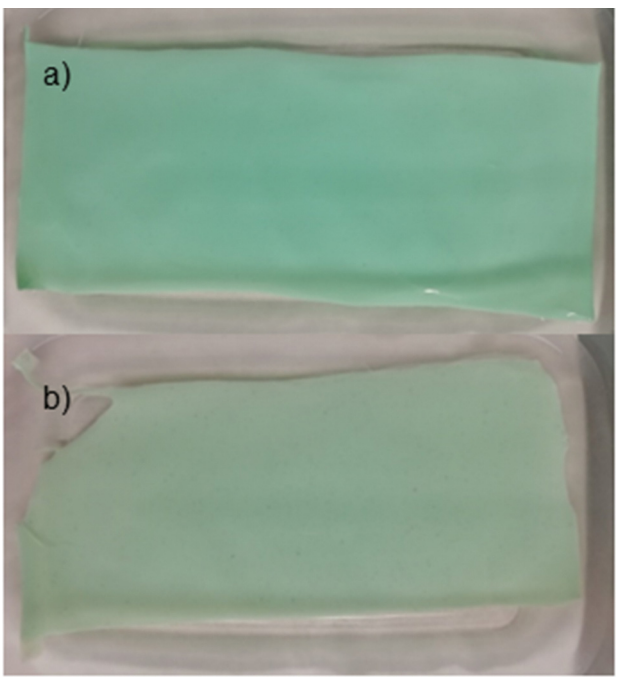

Fig. 12 Optical photographs of MMMs-bioMOFs containing bioMOFs $\{Ca^{II}Cu^{II}_6[(S,S)\text{-methox}]_3(OH)_2(H_2O)\}\cdot 16H_2O$ (a) and $\{Ca^{II}Cu^{II}_6[(S,S)\text{-Mecysmox}]_3(OH)_2(H_2O)\}\cdot 16H_2O$ (b). This figure is adapted with permission from ref. 77, copyright Wiley & Sons 2021.

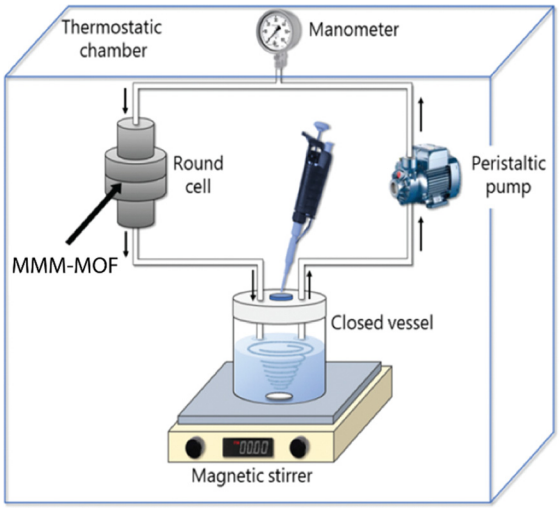

Scheme 2 Representation of the capture device for mercury decontamination. This figure is adapted with permission from ref. 77, copyright ACS 2022.

also followed another approach consisting on integrating our oxamidato-based bioMOFs with single-walled carbon nanotube buckypapers (bioMOF/SWCNT-BPs) (Fig. 13).[78,102] BPs are indeed suggested as innovative filtration systems, as an alternative to MMMs, given their well-known chemical resistance.[103–108] In particular, when combining oxamidato-based bioMOFs **Cu_6Ca-Met/Mecys** and also another bioMOF derived from amino acid L-threonine, with formula $\{Sr^{II}Cu^{II}_6[(S,S)\text{-threomox}]_3(OH)_2(H_2O)\}\cdot 36H_2O$ (**Cu6SrThreo**), with SWCNT-BPs, the resulting bioMOF/SWCNT-BPs exhibited excellent capture performances in Pb^{2+} capture[78] and Ce^{3+} recovery,[102] respectively. Overall, these findings serve as a proof-of-concept feasibility study and pave the way for new approaches in the development and application of bioMOF-carbon-based materials for recovery and environmental remediation, and eventually, their integration in water remediation devices.

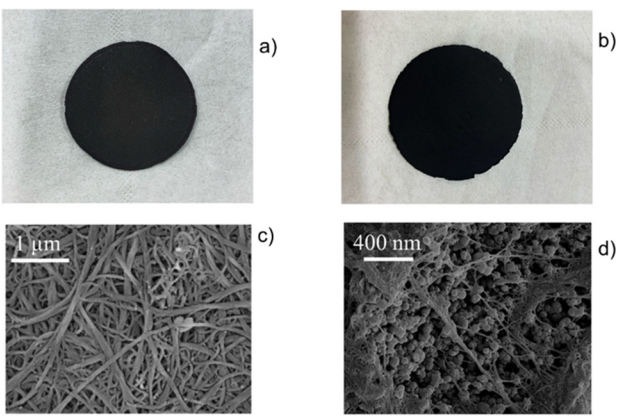

Fig. 13 Photographs of neat SWCNT-BP (a) and bioMOF@SWCNT-BP obtained by integrating **Cu_6SrThreo** and SWCNT-BP (b) circular membranes own an average diameter of 41 ± 1 mm. SEM images of SWCNT-BP (c) and bioMOF@SWCNT-BP (d). This figure is reproduced with permission from ref. 78, copyright ACS 2022.

5. Perspectives for oxamidato-based bioMOFs in real environments decontamination

Considering all the points discussed above, the great potential of oxamidato-based bioMOFs in environmental decontamination is evident. However, it is true that all experiments have been conducted at a laboratory scale so far, and a series of challenges must be overcome for their potential application in a real-world environment. For instance, it is essential to optimise the syntheses of oxamidato-based bioMOFs in order to minimise solvent, energy, and human resource consumption, making these processes economically viable. Additionally, it is extremely important to scale them up, once optimised, to produce large quantities of bioMOFs, preferably in a continuous manner. Secondly, oxamidato-based bioMOFs should be processed at large-scale into membranes, composites or sponges/foams, which, ultimately, could be used as filters in efficient and scalable capture devices. Last but not least, the efforts to design new MOFs must continue, so this bioMOF family could grow and they could effectively address the removal of novel emerging contaminants.

5.1. Synthesis optimisation and scale-up of oxamidato-based bioMOFs

Oxamidato-based bioMOFs are usually prepared following a three-step synthetic process: (i) preparation of the oxamidato ligand (Scheme 1a) from the selected amino acids, (ii) preparation and isolation of respective dicopper(II) complex (Scheme 1b) and (iii) formation of the target bioMOF (Scheme 1c) by coordination to a second metal (Ca^{II}, Sr^{II} or Ba^{II}). Among them, the second step is critical and hampers the economic viability of these materials, as it consumes large amounts of energy, time, solvents, and human resources. Therefore, it is essential to optimise this synthesis, preferably by eliminating this second stage and forming the bioMOFs directly in one-pot from the ligand. This would not only improve economic viability, but also, greatly facilitate the scaling-up of these materials.

In this context, it is fair to mention that oxamidato-based bioMOFs are particularly suitable to be scaled-up, as they precipitate at room temperature in one-pot syntheses in water and, in fact, can be easily obtained in a gram-scale, which contrasts to other methods in MOFs syntheses like solvothermal ones. These characteristics suggest that using large-scale chemical reactors should enable the production of these bioMOFs on a large scale. Alternatively, large-scale and continuous production methods, such as spray drying under continuous flow, would be interesting to be considered.

5.2. Shaping of oxamidato-based bioMOFs and incorporation in capture devices

With the ultimate goal of applying these materials in real-world environments, we have already mentioned in Section 4 that oxamidato-based bioMOFs must be processed in order to be used as filters in scalable capture devices and even in large

water treatment facilities. Indeed, we have previously described how bioMOFs can be incorporated into MMMs or SWCNT-BPs, maintaining excellent capture properties. Moreover, these composites can be incorporated on small-scale capture devices capable to decontaminate small amounts of aqueous solutions in a continuous flow.

In this context, it would be highly desirable to develop hybrid materials that incorporate our bioMOFs and could exhibit mechanical properties that allow them to withstand the flow of large volumes of contaminated water, while maintaining their capture capabilities. In this regard, based on a number of published results, we believe that a new type of composite, consisting of the combination of bioMOFs with functionalised cellulose foams, is highly promising. This composite would combine great mechanical strength and chemical versatility with the capture properties of both the bioMOFs and the substrate.

5.3. Design of novel examples of oxamidato-based (MTV)-bioMOFs

As a final remark, despite the high decontamination efficiency of the oxamidato-based bioMOFs described here, it is necessary to continue designing novel examples that can effectively address any emerging contaminants that may arise. In this regard, we believe that the development of new MTV-bioMOFs is the most appropriate strategy, not only due to their ability to simultaneously capture contaminants of diverse nature, but also to enhance the capture of pollutants with different functional groups.

A very illustrative example of emerging contaminant is represented by the so-called per- and polyfluoroalkyl substances (PFAS).[109] These species – ubiquitously present in the environment – are inefficiently removed by current remediation technologies, because of their particular physicochemical properties and the resulting intermolecular interactions that they can establish as a consequence of their dual hydrophobic/hydrophilic nature. On this basis, we speculate that the design of a MTV-bioMOF with both hydrophobic/hydrophilic functional groups should be suitable to capture efficiently a wide range of this type of molecules (Fig. 14).

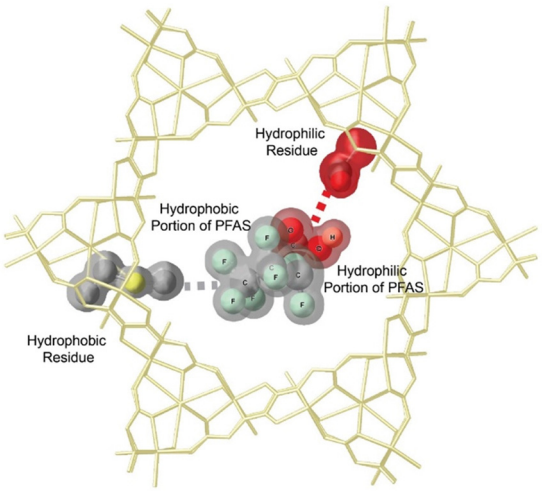

Fig. 14 Schematic representation of the capture mechanism suggested for MTV-bioMOFs towards PFAS.

6. Conclusions

In summary, in this feature article we have provided the reader with a comprehensive overview of some of the goodness reported in the recent years in oxamidato-based bioMOFs by our research group for the removal of contaminants from water. Great advances have been obtained with this quite novel family of bioMOFs, but these would be just academic exercises if we do not think in a global and holistic manner. For this reason, we have also developed a critical view of some of the main future steps needed to be addressed to be able to translate the basic knowledge reported in the highlighted manuscripts to real-world applications. Based on the presented results, we would like to reaffirm several distinguishable aspects of the unique potential of this family of bioMOFs, where besides their great removal performances, reusability and durability, we could rationalise most of these results with the beautiful insight of SCXRD, which is something quite unique even within MOFs field. This is also accompanied by the environmentally friendly nature and wide availability of constituting components, as well as the simplicity and eco-character of synthetic procedure, which is something to have in consideration toward the aimed sustainable development modern societies would have to face more seriously in the following decades. To sum up and finish, we would like to take the licence to give the reader the following message to take home: MTV-bioMOFs have supposed a sparkling revolution in materials chemistry for water remediation, oxamidato-based ones are just the simple vehicle we take advantage to enjoy and explore beyond the limits of knowledge with the ultimate aim to give back a substantial benefit to humanity and guarantee the sustainability of water ecosystems. But certainly, novel systems are waiting to be discovered, it is just a matter of time.

Author contributions

E. P. and T. G. wrote the first draft of the manuscript, and all the authors revised the draft and approved the final version of the manuscript.

Data availability

No primary research results, software or codes have been included as part of this review. All Figures (except Fig. 1) in the manuscript are newly prepared or adapted/reproduced with permission from the corresponding editorials. Image of Fig. 1 has been generated using Microsoft Designer.

Conflicts of interest

There are no conflicts to declare.

Acknowledgements

This work was supported by the Ministero dell'Istruzione, dell'Università e della Ricerca (Italy) and the MICINN (Spain) (Project PID2022-136349OB-I00 and Excellence Unit ''Maria de Maeztu'' CEX2019–000919–M). D. A. also acknowledges the financial support of the European Union – NextGenerationEU under the National Recovery and Resilience Plan (NRRP) of Ministero dell'Università e della Ricerca (MUR) (Project code PE0000021, ''Network 4 Energy Sustainable Transition'' – NEST). Thanks are also extended to the ''Generalitat Valenciana'' (Project PROMETEO/2021/054). E. P. acknowledges the financial support of the European Research Council under the European Union's Horizon 2020 research and innovation programme/ERC Grant Agreement No. 814804, MOF–reactors. Thanks are also extended to the Ramón y Cajal Program, RYC2019-027940-I (J. F.-S.). This study forms part of the Advanced Materials programme (MFA/2022/048) and was supported by MCIN with funding from European Union NextGenerationEU (PRTR-C17.I1) and by Generalitat Valenciana.

Notes and references

1 I. Vasilachi, D. Asiminicesei, D. Fertu and M. Gavrilescu, *Water*, 2021, **13**, 181.
2 D. Bunke, S. Moritz, W. Brack, D. L. Herráez, L. Posthuma and M. Nuss, *Environ. Sci. Eur.*, 2019, **31**, 32.
3 P. K. Rai, S. S. Lee, M. Zhang, Y. F. Tsang and K.-H. Kim, *Environ. Int.*, 2019, **125**, 365–385.
4 S.-M. Banyoi, T. Porseryd, J. Larsson, M. Grahn and P. Dinnétz, *Environ. Pollut.*, 2022, **315**, 120422.
5 D. Cheng, H. H. Ngo, W. Guo, S. W. Chang, D. D. Nguyen, Y. Liu, Q. Wei and D. Wei, *J. Hazard. Mater.*, 2020, **387**, 121682.
6 C. S. Skaggs and B. A. Logue, *Environ. Toxicol. Chem.*, 2022, **41**, 2658–2666.
7 K. Ulucan-Altuntas, N. Manav-Demir, F. Ilhan, H. B. Gelgor, K. Huddersman, A. Tiwary and E. Debik, *J. Water Process Eng.*, 2023, **51**, 103336.
8 N. H. Tran, M. Reinhard and K. Y.-H. Gin, *Water Res.*, 2018, **133**, 182–207.
9 S. R. Qasim, *Wastewater Treatment Plants*, Routledge, 2017.
10 F. R. Spellman, *Handbook of Water and Wastewater Treatment Plant Operations*, CRC Press, 2008.
11 A. S. Ruhl, F. Zietzschmann, I. Hilbrandt, F. Meinel, J. Altmann, A. Sperlich and M. Jekel, *Chem. Eng. J.*, 2014, **257**, 184–190.
12 H.-C. Zhou, J. R. Long and O. M. Yaghi, *Chem. Rev.*, 2012, **112**, 673–674.
13 H. Furukawa, K. E. Cordova, M. O'Keeffe and O. M. Yaghi, *Science*, 2013, **341**, 974.
14 H.-C. Zhou and S. Kitagawa, *Chem. Soc. Rev.*, 2014, **43**, 5415–5418.
15 X. Xiao, Y. Yu, Y. Sun, X. Zheng and A. Chen, *J. Environ. Sci.*, 2021, **108**, 22–32.
16 Z. Yang, P.-F. Sun, X. Li, B. Gan, L. Wang, X. Song, H.-D. Park and C. Y. Tang, *Environ. Sci. Technol.*, 2020, **54**, 15563–15583.
17 S. Bolisetty, M. Peydayesh and R. Mezzenga, *Chem. Soc. Rev.*, 2019, **48**, 463–487.
18 H. K. Chae, D. Y. Siberio-Pérez, J. Kim, Y. Go, M. Eddaoudi, A. J. Matzger, M. O'Keeffe and O. M. Yaghi, *Nature*, 2004, **427**, 523–527.
19 Y. Inokuma, M. Kawano and M. Fujita, *Nat. Chem.*, 2011, **3**, 349–358.
20 Z. Ji, H. Wang, S. Canossa, S. Wuttke and O. M. Yaghi, *Adv. Funct. Mater.*, 2020, **30**, 2000238.
21 M. Mon, R. Bruno, J. Ferrando-Soria, L. Bartella, L. Di Donna, M. Talia, R. Lappano, M. Maggiolini, D. Armentano and E. Pardo, *Mater. Horiz.*, 2018, **5**, 683–690.
22 A. Helal, Z. H. Yamani, K. E. Cordova and O. M. Yaghi, *Natl. Sci. Rev.*, 2017, **4**, 296–298.
23 T. M. Osborn Popp and O. M. Yaghi, *Acc. Chem. Res.*, 2017, **50**, 532–534.
24 M. Viciano-Chumillas, X. Liu, A. Leyva-Pérez, D. Armentano, J. Ferrando-Soria and E. Pardo, *Coord. Chem. Rev.*, 2022, **451**, 214273.
25 M. Mon, R. Bruno, J. Ferrando-Soria, D. Armentano and E. Pardo, *J. Mater. Chem. A*, 2018, **6**, 4912–4947.
26 E. M. Dias and C. Petit, *J. Mater. Chem. A*, 2015, **3**, 22484–22506.
27 D. Jiang, M. Chen, H. Wang, G. Zeng, D. Huang, M. Cheng, Y. Liu, W. Xue and Z. Wang, *Coord. Chem. Rev.*, 2019, **380**, 471–483.
28 S. Rojas and P. Horcajada, *Chem. Rev.*, 2020, **120**, 8378–8415.
29 B. Parmar, K. K. Bisht, G. Rajput and E. Suresh, *Dalton Trans.*, 2021, **50**, 3083–3108.
30 Y. Wen, P. Zhang, V. K. Sharma, X. Ma and H.-C. Zhou, *Cell Rep. Phys. Sci.*, 2021, **2**, 100348.
31 Q. Gao, J. Xu and X.-H. Bu, *Coord. Chem. Rev.*, 2019, **378**, 17–31.
32 A. C. McKinlay, R. E. Morris, P. Horcajada, G. Férey, R. Gref, P. Couvreur and C. Serre, *Angew. Chem., Int. Ed.*, 2010, **49**, 6260–6266.
33 I. Imaz, M. Rubio-Martínez, J. An, I. Solé-Font, N. L. Rosi and D. Maspoch, *Chem. Commun.*, 2011, **47**, 7287–7302.
34 P. A. Kobielska, A. J. Howarth, O. K. Farha and S. Nayak, *Coord. Chem. Rev.*, 2018, **358**, 92–107.
35 J. Li, X. Wang, G. Zhao, C. Chen, Z. Chai, A. Alsaedi, T. Hayat and X. Wang, *Chem. Soc. Rev.*, 2018, **47**, 2322–2356.
36 R. J. Drout, L. Robison, Z. Chen, T. Islamoglu and O. K. Farha, *Trends Chem.*, 2019, **1**, 304–317.
37 D. K. Yoo, B. N. Bhadra and S. H. Jhung, *J. Hazard. Mater.*, 2021, **403**, 123655.
38 X. Liu, Y. Shan, S. Zhang, Q. Kong and H. Pang, *Green Energy Environ.*, 2023, **8**, 698–721.
39 P. Kumar, V. Bansal, K.-H. Kim and E. E. Kwon, *J. Ind. Eng. Chem.*, 2018, **62**, 130–145.
40 T. Paul, A. Juma, R. Alqerem, G. Karanikolos, H. A. Arafat and L. F. Dumée, *J. Environ. Chem. Eng.*, 2023, **11**, 111112.
41 Q. Ma, T. Zhang and B. Wang, *Matter*, 2022, **5**, 1070–1091.
42 Z. Wang, L. Liu, Z. Li, N. Goyal, T. Du, J. He and G. K. Li, *Energy Fuels*, 2022, **36**, 2927–2944.
43 U. Ryu, S. Jee, P. C. Rao, J. Shin, C. Ko, M. Yoon, K. S. Park and K. M. Choi, *Coord. Chem. Rev.*, 2021, **426**, 213544.
44 M. Jaya Rajan and C. Indira Anish, *Water Quality - New Perspectives*, IntechOpen, 2024.
45 E. Pardo, R. Ruiz-García, J. Cano, X. Ottenwaelder, R. Lescouëzec, Y. Journaux, F. Lloret and M. Julve, *Dalton Trans.*, 2008, 2780.
46 M.-C. Dul, E. Pardo, R. Lescouëzec, Y. Journaux, J. Ferrando-Soria, R. Ruiz-García, J. Cano, M. Julve, F. Lloret, D. Cangussu, C. L. M. Pereira, H. O. Stumpf, J. Pasán and C. Ruiz-Pérez, *Coord. Chem. Rev.*, 2010, **254**, 2281–2296.
47 M. Viciano-Chumillas, M. Mon, J. Ferrando-Soria, A. Corma, A. Leyva-Pérez, D. Armentano and E. Pardo, *Acc. Chem. Res.*, 2020, **53**, 520–531.
48 R. J. Young, M. T. Huxley, E. Pardo, N. R. Champness, C. J. Sumby and C. J. Doonan, *Chem. Sci.*, 2020, **11**, 4031–4050.
49 M. Mon, J. Ferrando-Soria, T. Grancha, F. R. Fortea-Pérez, J. Gascon, A. Leyva-Pérez, D. Armentano and E. Pardo, *J. Am. Chem. Soc.*, 2016, **138**, 7864–7867.
50 F. R. Fortea-Pérez, M. Mon, J. Ferrando-Soria, M. Boronat, A. Leyva-Pérez, A. Corma, J. M. Herrera, D. Osadchii, J. Gascon, D. Armentano and E. Pardo, *Nat. Mater.*, 2017, **16**, 760–766.
51 M. Mon, J. Ferrando-Soria, M. Verdaguer, C. Train, C. Paillard, B. Dkhil, C. Versace, R. Bruno, D. Armentano and E. Pardo, *J. Am. Chem. Soc.*, 2017, **139**, 8098–8101.
52 M. Tejeda-Serrano, M. Mon, B. Ross, F. Gonell, J. Ferrando-Soria, A. Corma, A. Leyva-Pérez, D. Armentano and E. Pardo, *J. Am. Chem. Soc.*, 2018, **140**, 8827–8832.
53 M. A. Rivero-Crespo, M. Mon, J. Ferrando-Soria, C. W. Lopes, M. Boronat, A. Leyva-Pérez, A. Corma, J. C. Hernández-Garrido, M. López-Haro, J. J. Calvino, E. V. Ramos-Fernandez, D. Armentano and E. Pardo, *Angew. Chem., Int. Ed.*, 2018, **57**, 17094–17099.
54 M. Mon, M. A. Rivero-Crespo, J. Ferrando-Soria, A. Vidal-Moya, M. Boronat, A. Leyva-Pérez, A. Corma, J. C. Hernández-Garrido, M. López-Haro, J. J. Calvino, G. Ragazzon, A. Credi, D. Armentano and E. Pardo, *Angew. Chem., Int. Ed.*, 2018, **57**, 6186–6191.

55 M. Mon, R. Bruno, S. Sanz-Navarro, C. Negro, J. Ferrando-Soria, L. Bartella, L. Di Donna, M. Prejanò, T. Marino, A. Leyva-Pérez, D. Armentano and E. Pardo, *Nat. Commun.*, 2020, **11**, 3080.
56 J. Ballesteros-Soberanas, N. Martín, M. Bacic, E. Tiburcio, M. Mon, J. C. Hernández-Garrido, C. Marini, M. Boronat, J. Ferrando-Soria, D. Armentano, E. Pardo and A. Leyva-Pérez, *Nat. Catal.*, 2024, **7**, 452–463.
57 Z. Hasan and S. H. Jhung, *J. Hazard. Mater.*, 2015, **283**, 329–339.
58 P. W. Seo, J. Y. Song and S. H. Jhung, *Appl. Chem. Eng.*, 2016, **27**, 358–365.
59 N. A. Khan and S. H. Jhung, *J. Hazard. Mater.*, 2017, **325**, 198–213.
60 I. Ahmed, T. Panja, N. A. Khan, M. Sarker, J.-S. Yu and S. H. Jhung, *ACS Appl. Mater. Interfaces*, 2017, **9**, 10276–10285.
61 B. Hashemi, P. Zohrabi, N. Raza and K.-H. Kim, *TrAC, Trends Anal. Chem.*, 2017, **97**, 65–82.
62 C. Wang, X. Liu, N. Keser Demir, J. P. Chen and K. Li, *Chem. Soc. Rev.*, 2016, **45**, 5107–5134.
63 C. Xiao, J. Tian, Q. Chen and M. Hong, *Chem. Sci.*, 2024, **15**, 1570–1610.
64 J. Ferrando-Soria, P. Serra-Crespo, M. de Lange, J. Gascon, F. Kapteijn, M. Julve, J. Cano, F. Lloret, J. Pasán, C. Ruiz-Pérez, Y. Journaux and E. Pardo, *J. Am. Chem. Soc.*, 2012, **134**, 15301.
65 J. Ferrando-Soria, R. Ruiz-García, J. Cano, S.-E. Stiriba, J. Vallejo, I. Castro, M. Julve, F. Lloret, P. Amorós, J. Pasán, C. Ruiz-Pérez, Y. Journaux and E. Pardo, *Chem. - Eur. J.*, 2012, **18**, 1608–1617.
66 T. Grancha, J. Ferrando-Soria, J. Cano, P. Amorós, B. Seoane, J. Gascon, M. Bazaga-García, E. R. Losilla, A. Cabeza, D. Armentano and E. Pardo, *Chem. Mater.*, 2016, **28**, 4608–4615.
67 F. Gándara and T. D. Bennett, *IUCrJ*, 2014, **1**, 563–570.
68 W. M. Bloch, N. R. Champness and C. J. Doonan, *Angew. Chem., Int. Ed.*, 2015, **54**, 12860–12867.
69 J. Martí-Rujas, *Dalton Trans.*, 2020, **49**, 13897–13916.
70 M. A. Soldatov, A. Martini, A. L. Bugaev, I. Pankin, P. V. Medvedev, A. A. Guda, A. M. Aboraia, Y. S. Podkovyrina, A. P. Budnyk, A. A. Soldatov and C. Lamberti, *Polyhedron*, 2018, **155**, 232–253.
71 L. Liu, D. Zhang, Y. Zhu and Y. Han, *Commun. Chem.*, 2020, **3**, 99.
72 E. Tiburcio, R. Greco, M. Mon, J. Ballesteros-Soberanas, J. Ferrando-Soria, M. López-Haro, J. C. Hernández-Garrido, J. Oliver-Meseguer, C. Marini, M. Boronat, D. Armentano, A. Leyva-Pérez and E. Pardo, *J. Am. Chem. Soc.*, 2021, **143**, 2581–2592.
73 R. Adam, M. Mon, R. Greco, L. H. G. Kalinke, A. Vidal-Moya, A. Fernandez, R. E. P. Winpenny, A. Doménech-Carbó, A. Leyva-Pérez, D. Armentano, E. Pardo and J. Ferrando-Soria, *J. Am. Chem. Soc.*, 2019, **141**, 10350–10360.
74 R. Greco, E. Tiburcio-Fortes, A. Fernandez, C. Marini, A. Vidal-Moya, J. Oliver-Meseguer, D. Armentano, E. Pardo, J. Ferrando-Soria and A. Leyva-Pérez, *Chem. - Eur. J.*, 2022, **28**, e202103781.
75 M. Mon, F. Lloret, J. Ferrando-Soria, C. Martí-Gastaldo, D. Armentano and E. Pardo, *Angew. Chem., Int. Ed.*, 2016, **55**, 11167–11172.
76 M. Mon, X. Qu, J. Ferrando-Soria, I. Pellicer-Carreño, A. Sepúlveda-Escribano, E. V. Ramos-Fernandez, J. C. Jansen, D. Armentano and E. Pardo, *J. Mater. Chem. A*, 2017, **5**, 20120–20125.
77 R. Bruno, M. Mon, P. Escamilla, J. Ferrando-Soria, E. Esposito, A. Fuoco, M. Monteleone, J. C. Jansen, R. Elliani, A. Tagarelli, D. Armentano and E. Pardo, *Adv. Funct. Mater.*, 2021, **31**, 2008499.
78 M. Baratta, T. F. Mastropietro, R. Bruno, A. Tursi, C. Negro, J. Ferrando-Soria, A. I. Mashin, A. Nezhdanov, F. P. Nicoletta, G. De Filpo, E. Pardo and D. Armentano, *ACS Appl. Nano Mater.*, 2022, **5**, 5223–5233.
79 M. Mon, R. Bruno, E. Tiburcio, P.-E. Casteran, J. Ferrando-Soria, D. Armentano and E. Pardo, *Chem. - Eur. J.*, 2018, **24**, 17712–17718.
80 C. Negro, P. Escamilla, R. Bruno, J. Ferrando-Soria, D. Armentano and E. Pardo, *Chem. - Eur. J.*, 2022, **28**, e202200034.
81 C. Negro, H. Martínez Pérez-Cejuela, E. F. Simó-Alfonso, J. M. Herrero-Martínez, R. Bruno, D. Armentano, J. Ferrando-Soria and E. Pardo, *ACS Appl. Mater. Interfaces*, 2021, **13**, 28424–28432.
82 C. Negro, H. Martínez Pérez-Cejuela, E. F. Simó-Alfonso, W. Iqbal, J. M. Herrero-Martínez, D. Armentano, J. Ferrando-Soria and E. Pardo, *ACS Appl. Mater. Interfaces*, 2023, **15**, 3069–3076.
83 M. Mon, R. Bruno, E. Tiburcio, M. Viciano-Chumillas, L. H. G. Kalinke, J. Ferrando-Soria, D. Armentano and E. Pardo, *J. Am. Chem. Soc.*, 2019, **141**, 13601–13609.
84 **https://www.who.int/water_sanitation_health/en/**.
85 S. Booth and D. Zeller, *Environ. Health Perspect.*, 2005, **113**, 521–526.
86 Y. Lin, Y. Yang, Y. Li, L. Yang, X. Hou, X. Feng and C. Zheng, *Environ. Sci. Technol.*, 2016, **50**, 2468–2476.
87 M. Feng, P. Zhang, H.-C. Zhou and V. K. Sharma, *Chemosphere*, 2018, **209**, 783–800.
88 P. Kumar, A. Pournara, K.-H. Kim, V. Bansal, S. Rapti and M. J. Manos, *Prog. Mater. Sci.*, 2017, **86**, 25–74.
89 T. Velempini and K. Pillay, *J. Environ. Chem. Eng.*, 2019, **7**, 103350.
90 K. J. Pieper, M. Tang and M. A. Edwards, *Environ. Sci. Technol.*, 2017, **51**, 2007–2014.
91 **https://www.who.int/teams/environment-climate-change-and-health/chemical-safety-and-health/health-impacts/chemicals/lead**.
92 **https://www.epa.gov/ground-water-and-drinking-water**.
93 P. Escamilla, M. Monteleone, R. M. Percoco, T. F. Mastropietro, M. Longo, E. Esposito, A. Fuoco, J. C. Jansen, R. Elliani, A. Tagarelli, J. Ferrando-Soria, V. Amendola, E. Pardo and D. Armentano, *ACS Appl. Mater. Interfaces*, 2024, **16**, 51182–51194.
94 S. Dutta, S. Adhikary, S. Bhattacharya, D. Roy, S. Chatterjee, A. Chakraborty, D. Banerjee, A. Ganguly, S. Nanda and P. Rajak, *J. Environ. Manage.*, 2024, **353**, 120103.
95 K. Maheshwari, M. Agrawal and A. B. Gupta, in *Novel Materials for Dye-containing Wastewater Treatment*, Springer Nature, 2021, pp. 1–25.
96 A. Tkaczyk, K. Mitrowska and A. Posyniak, *Sci. Total Environ.*, 2020, **717**, 137222.
97 M. Tudi, H. Daniel Ruan, L. Wang, J. Lyu, R. Sadler, D. Connell, C. Chu and D. T. Phung, *Int. J. Environ. Res. Public Health*, 2021, **18**, 1112.
98 E. F. S. Authority, *EFSA J.*, 2013, **11**, 3066.
99 **https://www.eea.europa.eu/en/analysis/indicators/pesticides-in-rivers-lakes-and**.
100 F. Yan, L. An, X. Xu, W. Du and R. Dai, *Sci. Total Environ.*, 2024, **906**, 167737.
101 H. M. Pérez-Cejuela, M. Mon, J. Ferrando-Soria, E. Pardo, D. Armentano, E. F. Simó-Alfonso and J. M. Herrero-Martínez, *Microchim. Acta*, 2020, **187**, 201.
102 A. Tursi, T. F. Mastropietro, R. Bruno, M. Baratta, J. Ferrando-Soria, A. I. Mashin, F. P. Nicoletta, E. Pardo, G. De Filpo and D. Armentano, *Adv. Mater. Interfaces*, 2021, **8**, 2100730.
103 B. Lee, Y. Baek, M. Lee, D. H. Jeong, H. H. Lee, J. Yoon and Y. H. Kim, *Nat. Commun.*, 2015, **6**, 1–7.
104 A. Khalid, A. A. Al-Juhani, O. C. Al-Hamouz, T. Laoui, Z. Khan and M. A. Atieh, *Desalination*, 2015, **367**, 134–144.
105 H. Y. Yang, Z. J. Han, S. F. Yu, K. L. Pey, K. Ostrikov and R. Karnik, *Nat. Commun.*, 2013, **4**, 2220.
106 K. C. Khulbe and T. Matsuura, *Appl. Water Sci.*, 2018, **8**, 1–30.
107 Ihsanullah, *Sep. Purif. Technol.*, 2019, **209**, 307–337.
108 B. Ribeiro, L. F. P. Santos, A. L. Santos, M. L. Costa and E. C. Botelho, *J. Thermoplast. Compos. Mater.*, 2019, **32**, 62–75.
109 T. F. Mastropietro, R. Bruno, E. Pardo and D. Armentano, *Dalton Trans.*, 2021, **50**, 5398–5410.